the L205R mutation enhanced the phosphorylation catalysis of PKA.

The identification of activating mutations in oncogenes is particularly valuable in developing targeted therapies for cancer. PKA signaling plays a pivotal role in various physiological and pathological processes, including development, metabolism, and tumorigenesis. Although inactivating mutations in *PRKAR1A* and phosphodiesterase genes are known in adrenal hyperplasia, we revealed the activating *PRKACA* L205R mutation and several potential functional mutated genes in ACTs. Future investigations on mutagenesis and hormones or environmental initiators of the L205R mutation may provide clues for prevention or treatment of Cushing's syndrome.

REFERENCES AND NOTES

1. J. Newell-Price, X. Bertagna, A. B. Grossman, L. K. Nieman, *Lancet* **367**, 1605–1617 (2006).
2. C. A. Stratakis, S. A. Boikos, *Nat. Clin. Pract. Endocrinol. Metab.* **3**, 748–757 (2007).
3. L. S. Kirschner *et al.*, *Nat. Genet.* **26**, 89–92 (2000).
4. See supplementary materials on *Science* Online.
5. A. Berthon, A. Martinez, J. Bertherat, P. Val, *Mol. Cell. Endocrinol.* **351**, 87–95 (2012).
6. S. Gaujoux *et al.*, *Clin. Cancer Res.* **16**, 5133–5141 (2010).
7. L. S. Weinstein *et al.*, *N. Engl. J. Med.* **325**, 1688–1695 (1991).
8. M. C. Fragoso *et al.*, *J. Clin. Endocrinol. Metab.* **88**, 2147–2151 (2003).
9. J. Min, Q. Feng, Z. Li, Y. Zhang, R.-M. Xu, *Cell* **112**, 711 (2003).
10. Y. Okada *et al.*, *Cell* **121**, 167–178 (2005).
11. G. Assié *et al.*, *N. Engl. J. Med.* **369**, 2105–2114 (2013).
12. N. Galjart, *Nat. Rev. Mol. Cell Biol.* **6**, 487–498 (2005).
13. M. D. Uhler *et al.*, *Proc. Natl. Acad. Sci. U.S.A.* **83**, 1300–1304 (1986).
14. B. Nolen, S. Taylor, G. Ghosh, *Mol. Cell* **15**, 661–675 (2004).
15. P. Madhusudan, P. Akamine, N. H. Xuong, S. S. Taylor, *Nat. Struct. Biol.* **9**, 273–277 (2002).
16. M. J. Moore, J. A. Adams, S. S. Taylor, *J. Biol. Chem.* **278**, 10613–10618 (2003).
17. J. Yang, L. F. Ten Eyck, N. H. Xuong, S. S. Taylor, *J. Mol. Biol.* **336**, 473–487 (2004).
18. J. Yang *et al.*, *J. Mol. Biol.* **346**, 191–201 (2005).
19. C. Kim, N. H. Xuong, S. S. Taylor, *Science* **307**, 690–696 (2005).
20. C. Kim, C. Y. Cheng, S. A. Saldanha, S. S. Taylor, *Cell* **130**, 1032–1043 (2007).
21. D. Sarkar *et al.*, *J. Clin. Endocrinol. Metab.* **86**, 1653–1659 (2001).
22. S. Acharyya *et al.*, *Cell* **150**, 165–178 (2012).
23. E. Meimaridou *et al.*, *Endocr. Dev.* **24**, 57–66 (2013).
24. D. Lin *et al.*, *Science* **267**, 1828–1831 (1995).
25. P. R. Manna, M. T. Dyson, D. M. Stocco, *Mol. Hum. Reprod.* **15**, 321–333 (2009).
26. S. S. Taylor, R. Ilouz, P. Zhang, A. P. Kornev, *Nat. Rev. Mol. Cell Biol.* **13**, 646–658 (2012).

ACKNOWLEDGMENTS

Supported by Natural Science Foundation of China grants 30900702, 81130016, and 81270859, and by Guangdong Innovative Research Team Program grant 2009010016. The sequencing data have been deposited in the European Genome-phenome Archive (accession no. EGAS00001000712).

SUPPLEMENTARY MATERIALS

www.sciencemag.org/content/344/6186/913/suppl/DC1
Materials and Methods
Figs. S1 to S8
Tables S1 to S11
References (*27–40*)

9 December 2013; accepted 21 March 2014
Published online 3 April 2014;
10.1126/science.1249480

CANCER GENOMICS

Recurrent somatic mutations underlie corticotropin-independent Cushing's syndrome

Yusuke Sato,[1,2]* Shigekatsu Maekawa,[2]* Ryohei Ishii,[3] Masashi Sanada,[1] Teppei Morikawa,[4] Yuichi Shiraishi,[5] Kenichi Yoshida,[1] Yasunobu Nagata,[1] Aiko Sato-Otsubo,[1] Tetsuichi Yoshizato,[1] Hiromichi Suzuki,[1] Yusuke Shiozawa,[1] Keisuke Kataoka,[1] Ayana Kon,[1] Kosuke Aoki,[1] Kenichi Chiba,[5] Hiroko Tanaka,[6] Haruki Kume,[2] Satoru Miyano,[5,6] Masashi Fukayama,[4] Osamu Nureki,[3] Yukio Homma,[2]† Seishi Ogawa[1]†

Cushing's syndrome is caused by excess cortisol production from the adrenocortical gland. In corticotropin-independent Cushing's syndrome, the excess cortisol production is primarily attributed to an adrenocortical adenoma, in which the underlying molecular pathogenesis has been poorly understood. We report a hotspot mutation (L206R) in *PRKACA*, which encodes the catalytic subunit of cyclic adenosine monophosphate (cAMP)–dependent protein kinase (PKA), in more than 50% of cases with adrenocortical adenomas associated with corticotropin-independent Cushing's syndrome. The L206R PRKACA mutant abolished its binding to the regulatory subunit of PKA (PRKAR1A) that inhibits catalytic activity of PRKACA, leading to constitutive, cAMP-independent PKA activation. These results highlight the major role of cAMP-independent activation of cAMP/PKA signaling by somatic mutations in corticotropin-independent Cushing's syndrome, providing insights into the diagnosis and therapeutics of this syndrome.

Cushing's syndrome is a systemic disorder associated with various constitutive symptoms—such as hypertension, impaired glucose tolerance, central obesity, osteoporosis, and depression—that are ascribed to cortisol overproduction (*1–3*). Cortisol biosynthesis is primarily regulated by corticotropin secreted from the anterior pituitary gland. Corticotropin acts by binding to the melanocortin-2 receptor, increases cyclic adenosine monophosphate (cAMP) production, and activates cAMP-dependent protein kinase [protein kinase A (PKA)] (*4*). While aberrant corticotropin secretion from pituitary adenoma or other ectopic sites is the leading cause of Cushing's syndrome (corticotropin-dependent Cushing's syndrome), excess cortisol is autonomously produced by adrenocortical tumors in patients with corticotropin-independent Cushing's syndrome (*2*, *5*, *6*). Although mutations in the regulatory subunit type I alpha of PKA (*PRKAR1A*) (*7*, *8*) guanine nucleotide-binding protein subunit alpha (*GNAS*) (*9*), phosphodiesterase-8B (*PDE8B*) (*10*, *11*) and -11A (*PDE11A*) (*12*), and armadillo repeat containing 5 (*ARMC5*) (*13*) are responsible for rare syndromic or hereditary disorders with bilateral adrenocortical hyperplasia, molecular pathogenesis of cortisol-producing adrenocortical adenomas, which account for a large portion of corticotropin-independent Cushing's syndrome (*6*), are less studied.

To investigate genetic lesions in corticotropin-independent Cushing's syndrome, we performed whole-exome sequencing (WES) of eight adrenocortical tumors and matched normal specimens (fig. S1 and table S1). We identified a total of 45 validated nonsynonymous and 59 putative synonymous somatic mutations (tables S2 and S3) (see the supplementary materials). Remarkably, the gene encoding the catalytic subunit (C subunit) of PKA (*PRKACA*) was recurrently mutated in four out of the eight cases, resulting in an identical c.T617G mutation predicted to cause a conversion of leucine to arginine at amino acid position 206 (p.L206R). Together with a *GNAS* mutation (p.R201C), five of the eight cases had somatic mutations in genes involved in the cAMP/PKA signaling pathway. No allelic imbalances were observed at both gene loci in single-nucleotide polymorphism (SNP) array analysis (fig. S2), indicating that these mutations were heterozygous, which was consistent with the observation that, in exome sequencing, variant allele frequencies (VAF) of *PRKACA*/*GNAS* mutations were comparable to those of other somatic mutations (fig. S3). Mutations were not detected in any other known causative genes, including *PRKAR1A*, *PDE11A*, *PDE8B*, and *ARMC5*.

[1]Department of Pathology and Tumor Biology, Graduate School of Medicine, Kyoto University, Kyoto, Japan. [2]Department of Urology, Graduate School of Medicine, The University of Tokyo, Tokyo, Japan. [3]Department of Biophysics and Biochemistry, Graduate School of Science, The University of Tokyo, Tokyo, Japan. [4]Department of Pathology, Graduate School of Medicine, The University of Tokyo, Tokyo, Japan. [5]Laboratory of DNA Information Analysis, Human Genome Center, Institute of Medical Science, The University of Tokyo, Tokyo, Japan. [6]Laboratory of Sequence Analysis, Human Genome Center, Institute of Medical Science, The University of Tokyo, Tokyo, Japan.
*These authors contributed equally to this work. †**Corresponding author. E-mail: sogawa-tky@umin.ac.jp (S.O.); homma-uro@umin.ac.jp (Y.H.)**

We performed follow-up sequencing of *PRKACA* and *GNAS* as well as previously reported genes (*PRKAR1A*, *PDE11A*, *PDE8B*, and *ARMC5*) in an additional 57 cases (see the supplementary materials). The L206R mutation in *PRKACA* was found in 30 out of the 57 follow-up cases, of which 24 cases were confirmed as being somatic, whereas *GNAS* mutations were found in 10 cases, with somatic origin being confirmed in six cases (table S1, Fig. 1, and fig. S4). No mutations were found in the previously reported genes. The eight samples double-negative for *PRKACA* and *GNAS* mutations were tested for mutations in seven additional genes that were mutated and expressed in three double-negative exome cases, but no more recurrent mutations were identified. Combined with the four *PRKACA* and one *GNAS* mutations in the discovery cases, *PRKACA* and *GNAS* were mutated in 34 (52.3%) and 11 (16.9%) out of the 65 cases with corticotropin-independent Cushing's syndrome, respectively, where both mutations were completely mutually exclusive (Fisher's exact test, $P = 9.46 \times 10^{-5}$) (Fig. 1). The somatic origin was confirmed for 28 out of 28 *PRKACA* and 6 out of 6 *GNAS* mutations thus far tested. In addition, VAFs of *PRKACA* and *GNAS* mutations in deep sequencing were distributed between 0.08 and 0.35, whereas those of most heterozygous SNPs (83%) were between 0.4 and 0.6 (fig. S5), indicating that most of these mutations were somatic in origin.

Patients with mutated *PRKACA* showed significantly higher cortisol levels on the 1-mg dexamethasone suppression test (DST) compared with wild-type *PRKACA* and *GNAS* (*t* test, $P = 2.60 \times 10^{-3}$) (Fig. 2A). *PRKACA*-mutated adenomas had a significantly smaller tumor diameter than those with no known mutations (*t* test, $P = 4.93 \times 10^{-5}$) (Fig. 2B), suggesting that *PRKACA*-mutated adenomas may have higher cortisol production. *GNAS*-mutated adenomas also showed higher cortisol levels on 1-mg DST and have a smaller tumor size. Seventy-six percent of the patients with clinical Cushing's syndrome had a mutation of either gene, whereas only two of nine patients with subclinical Cushing's syndrome had mutated *PRKACA* or *GNAS* genes (Fisher's exact test, $P = 2.87 \times 10^{-3}$) (Fig. 2C and table S4), indicating that these mutations were enriched for clinical Cushing's syndrome.

PRKACA is the catalytic (C) subunit of the tetrameric PKA holoenzyme, which binds tissue-specific dimeric regulatory (R) subunits (*14–16*). In the native state, the C subunit is kept inactivated through the binding of the R subunit, which masks the catalytic site of the C subunit (Fig. 3A). However, when intracellular cAMP is up-regulated by external stimuli, each R subunit binds two cAMP molecules, which causes a conformational change in the R subunit to promote dissociation of the C subunit from the PKA complex (*14–16*), allowing for the translocation of the dissociated, and thereby activated, free C subunit to the nucleus and phosphorylation of its target substrates therein (*17, 18*). The highly conserved L206 residue of PRKACA, which resides within the P+1 loop of the C subunit, lies on the surface of the large lobe of PRKACA and is thought to be essential for the catalytic activity of the kinase (Fig. 3A, and fig. S6) (*14–16*). In the absence of cAMP, the inhibitory region of the R subunit docks to the active site cleft of the C subunit, including the P+1 loop. The L206 residue is located at the interface between the C subunit and the inhibitory region in the R subunit to form a hydrophobic interaction with the I99 residue of the R subunit (Fig. 3B). Thus, the substitution from the small hydrophobic leucine to a large hydrophobic arginine is predicted to cause steric hindrance and abolish the binding of the C and R subunits (Fig. 3C), resulting in constitutive, cAMP-independent activation of PKA.

In fact, when the PKA complex was reconstituted in vitro using purified proteins (fig. S7), PRKAR1A binds the wild-type C subunit and suppresses its PKA activity in the absence of cAMP, and the suppression is recovered in the presence of cAMP with substantially reduced interaction with the wild-type C subunit (Fig. 4, A and B). In contrast, the R subunit can no longer bind the L206R PRKACA mutant with constitutive PKA activation, regardless of the presence or absence of cAMP (Fig. 4, A and B). The loss of binding to the R subunit and consequent cAMP-independent PKA activation for the mutant PRKACA was also demonstrated in vivo. When expressed in human embryonic kidney 293T (HEK293T) cells (fig. S8), wild-type PRKACA, but not the L206R PRKACA mutant, coimmunoprecipitated with PRKAR1A (Fig. 4C). Both mock- and wild-type *PRKACA*-transduced cells showed increased PKA activity accompanied by an elevated phosphorylation of cAMP response element–binding protein (pCREB), one of the major downstream targets of PKA activation (Fig. 4, D and E, and fig. S9), on cAMP induction by forskolin treatment (see the supplementary materials), whereas mutant *PRKACA*-transduced cells demonstrated a higher basal level of PKA activity and CREB phosphorylation, regardless of forskolin treatment (Fig. 4, D and E, and fig. S9). To confirm the cAMP-independent activation of the mutant PRKACA, we examined the effect of two PRKACA inhibitors (H89 and KT5720) and a competitive inhibitor of cAMP binding for the R subunit (Rp-cAMPS) on the activity of the L206R mutant (see the supplementary materials). PKA activation in the L206R mutant–transduced cells in the absence of forskolin was suppressed by H89 and KT5720 (*t* test, $P = 1.60 \times 10^{-3}$ and $P = 1.86 \times 10^{-3}$, respectively) but not in Rp-cAMPS–treated cells, supporting further that the consequence of the L206R mutation is constitutive, cAMP-independent activation of PKA (Fig. 4F and fig. S10).

Finally, as predicted from low stability of free C subunits, primary *PRKACA*-mutated tumors showed significantly lower PRKACA protein expression compared with unmutated tumors (*t* test, $P = 5.70 \times 10^{-3}$) and normal adrenocortical tissues (*t* test, $P = 2.09 \times 10^{-2}$) (Fig. 4G and fig. S11), although no significant difference was observed for downstream signaling, such as pCREB or steroidogenic acute regulatory protein (StAR). The reduced intracellular expression of the mutant PRKACA protein was also observed for

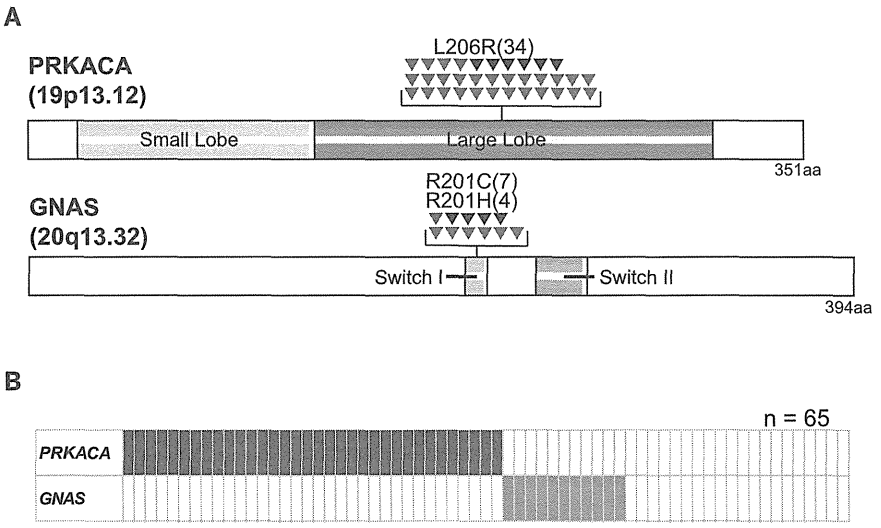

Fig. 1. Recurrent mutations in *PRKACA* and *GNAS*. (**A**) Mutations in *PRKACA* (top) and *GNAS* (bottom) identified in 65 patients with corticotropin-independent Cushing's syndrome (arrowheads). Confirmed somatic mutations are indicated in red. (**B**) Mutually exclusive distribution of *PRKACA* and *GNAS* mutations.

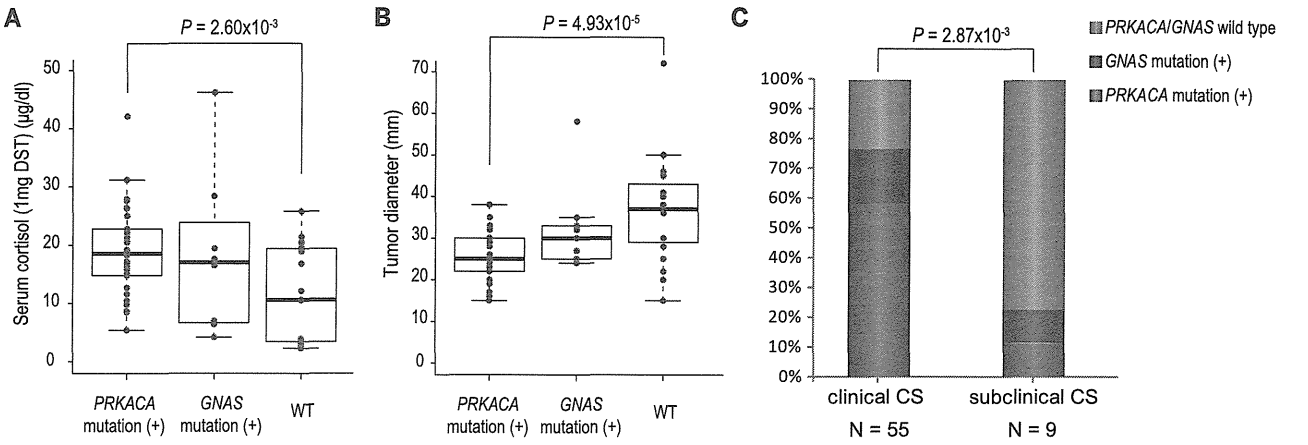

Fig. 2. Relationship between mutation status and clinical features. (**A** and **B**) Serum cortisol level of 1-mg dexamethasone (A) and the diameter of adrenocortical adenoma (B) according to the mutation status of *PRKACA*/*GNAS* genes. (**C**) Clinical and subclinical Cushing's syndrome as attributed to mutated *PRKACA*, *GNAS*, or other, currently undetected, cause.

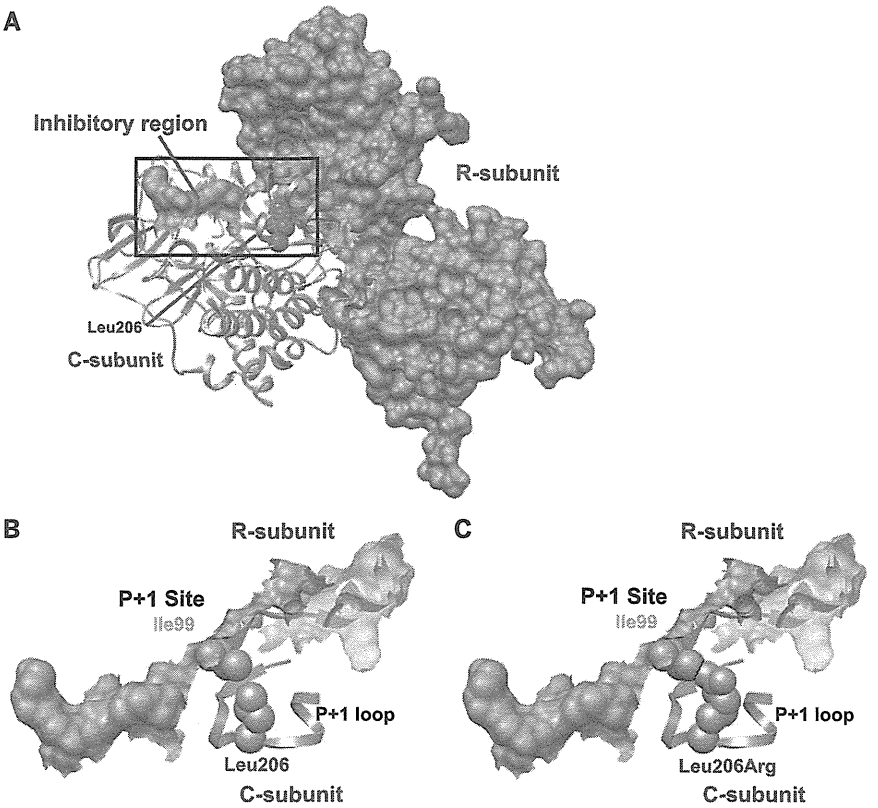

Fig. 3. Effect of L206R mutation on three-dimensional structures of PKA. (**A**) Three-dimensional structure of the PKA complex, composed of C (PRKACA) (pink) and R (PRKAR1A) (cyan) subunits, is depicted using the University of California–San Francisco Chimera program, based on the Research Collaboratory for Structural Bioinformatics Protein Data Bank (PDB ID: 2QCS). L206 is shown in red. (**B** and **C**) A predicted effect of the L206R mutation within the P+1 loop on the interaction with the R subunit (C) in comparison with wild-type PRKACA (B).

exogenously introduced PRKACA in different cell types (Fig. 4H and fig. S12). However, compared with the wild-type protein, mutant PRKACA was more enriched in the nuclear than in the cytoplasmic fraction (Fig. 4H).

In conclusion, frequent somatic mutations in *PRKACA* and *GNAS* genes underlie corticotropin-independent Cushing's syndrome (fig. S13). Strikingly, in accordance with a recent report (*19*) *PRKACA* mutations were found in more than 50% of the current cohort. All the mutations were the identical L206R substitution, which prevents binding to the inhibitory R subunits and results in constitutive, cAMP-independent activation of PKA. *GNAS* mutations were also detected in a substantial fraction of the present cohort (11/65 or 16.9%), in which all were confined to the R201 residue. Steroid hormone biosynthesis in steroidogenic cells is primarily regulated through activation of the cAMP/PKA signaling pathway (*20*). *PRKACA* and *GNAS* mutations in adrenocortical cells affecting this pathway are thus a likely factor responsible for the excessive production of cortisol and together account for as many as 70% of the current cohort of the patients. In contrast, the remaining 30% of the patients with no mutations in either gene tended to show lower cortisol levels on 1-mg DST and had a larger tumor size compared with *PRKACA*-mutated patients. In addition, the identified mutations were confined almost exclusively to patients with clinical Cushing's syndrome, suggesting that double-negative cases have distinct pathogenesis, with driver mutations still to be identified. It should be warranted to identify the genetic basis of double-negative cases in future studies.

Fig. 4. Functional characterization of PRKACA mutant. (**A**) Immunoblot analysis of antibody to FLAG immunoprecipitates of the PKA reconstructed in vitro with large-scale–purified proteins, in which PRKACA and PRKAR1A subunits are tagged with hemagglutinin (HA) and FLAG, respectively. (**B**) In vitro PKA activities of wild-type and mutant PRKACA in the presence or absence of PRKAR1A and cAMP with purified proteins. (**C**) Immunoblot analysis of the total cell lysates (input) and antibody to HA immunoprecipitates from HEK293T cells stably transduced with either mock, wild-type, or mutant PRKACA tagged with HA with indicated antibodies. (**D**) PKA activities in HEK293T cells stably transduced with either mock, wild-type, or mutant PRKACA in the presence or absence of forskolin stimulation. (**E**) Relative expression of pCREB to total CREB in HEK293T cells stably transduced with either mock, wild-type, or mutant PRKACA as determined by densitometry of the immunoblots. (**F**) The effect of inhibition of PKA (H89 and KT5720) and cAMP (Rp-cAMPS) in HEK293T cells transduced with mock or mutant PRKACA. (**G**) PRKACA expression standardized for mRNA expression in *PRKACA*-mutated and unmutated adenomas and matched normal adrenocortical tissues. (**H**) Western blot analysis of indicated fractions of cell lysates from wild-type and mutant PRKACA-transduced HEK293T cells using indicated antibodies. Standard errors and significant differences are indicated [(C) to (G)].

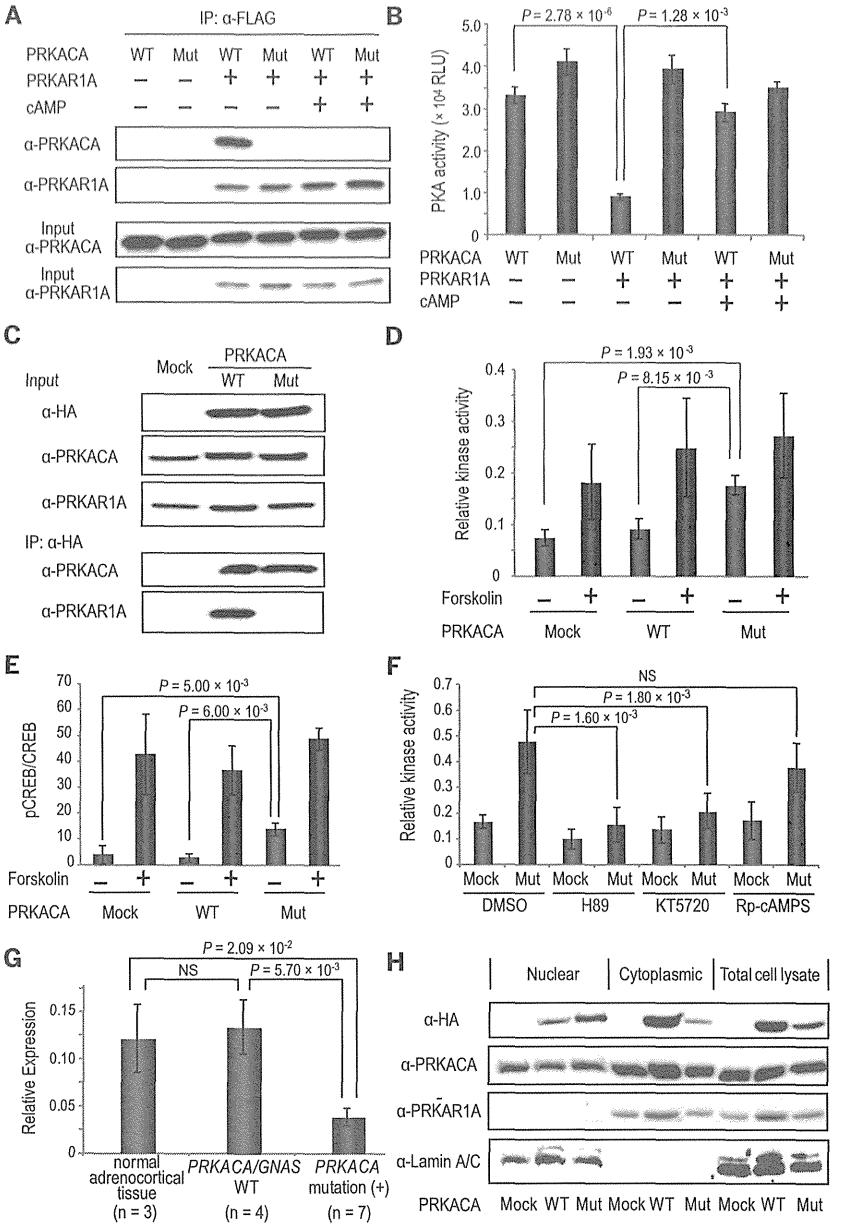

REFERENCES AND NOTES

1. L. K. Nieman *et al.*, *J. Clin. Endocrinol. Metab.* **93**, 1526–1540 (2008).
2. B. A. Hatipoglu, *J. Surg. Oncol.* **106**, 565–571 (2012).
3. J. Newell-Price, X. Bertagna, A. B. Grossman, L. K. Nieman, *Lancet* **367**, 1605–1617 (2006).
4. K. G. Mountjoy, L. S. Robbins, M. T. Mortrud, R. D. Cone, *Science* **257**, 1248–1251 (1992).
5. D. N. Orth, *N. Engl. J. Med.* **332**, 791–803 (1995).
6. C. A. Stratakis, *Endocr. Dev.* **13**, 117–132 (2008).
7. L. S. Kirschner *et al.*, *Nat. Genet.* **26**, 89–92 (2000).
8. L. S. Kirschner *et al.*, *Hum. Mol. Genet.* **9**, 3037–3046 (2000).
9. L. S. Weinstein *et al.*, *N. Engl. J. Med.* **325**, 1688–1695 (1991).
10. A. Horvath *et al.*, *Nat. Genet.* **38**, 794–800 (2006).
11. A. Horvath *et al.*, *Cancer Res.* **66**, 11571–11575 (2006).
12. A. Horvath, V. Mericq, C. A. Stratakis, *N. Engl. J. Med.* **358**, 750–752 (2008).
13. G. Assié *et al.*, *N. Engl. J. Med.* **369**, 2105–2114 (2013).
14. M. J. Moore, J. A. Adams, S. S. Taylor, *J. Biol. Chem.* **278**, 10613–10618 (2003).
15. C. Kim, N. H. Xuong, S. S. Taylor, *Science* **307**, 690–696 (2005).
16. C. Kim, C. Y. Cheng, S. A. Saldanha, S. S. Taylor, *Cell* **130**, 1032–1043 (2007).
17. M. R. Montminy, L. M. Bilezikjian, *Nature* **328**, 175–178 (1987).
18. A. T. Harootunian *et al.*, *Mol. Biol. Cell* **4**, 993–1002 (1993).
19. F. Beuschlein *et al.*, *N. Engl. J. Med.* **370**, 1019–1028 (2014).
20. A. M. Lefrancois-Martinez *et al.*, *J. Biol. Chem.* **286**, 32976–32985 (2011).

ACKNOWLEDGMENTS

We thank Y. Mori, M. Nakamura, N. Mizota, S. Ichimura, and M. Yamakawa for their technical assistance. The retroviral vector, pGCDNsamIRES-EGFP, was kindly provided by M. Onodera (National Research Institute for Child Health and Development). This work was supported by the Japan Society for the Promotion of Science (JSPS) through Grants-in-Aid for Scientific Research (KAKENHI) grant number 22134006 and the Funding Program for World-Leading Innovative Research and Development on Science and Technology (FIRST Program). Data for exome sequencing, as well as SNP array analysis, are found in the European Genome-phenome Archive (EGA) under accession EGAS00001000661. Author contributions: Y.Sa., S.Ma., K.Y., Y.N., T.Y., H.S., and A.K. performed library preparation and DNA sequencing. Y.Shira., Y.Shio., K.C., H.T., and S.Mi. were committed to bioinformatics analyses of resequencing data. Y.Sa. and A.S.-O. performed SNP array analysis. Y.Sa., S.Ma., M.S., R.I., K.K., and O.N. performed the functional analyses of PRKACA mutant. T.M., H.K., M.F., and Y.H. provided specimens and were also involved in planning the project. Y.Sa., S.Ma., M.S., R.I., and S.O. generated figures and tables and wrote the manuscript. S.O. led the entire project. All authors participated in the discussion and interpretation of data and results. Y.Sa., S.Ma., M.S., Y.H., and S.O. are inventors on a patent applied for by Kyoto University that covers the inspection method for Cushing's syndrome and biomarker and theraputic agent thereof (2014-37189).

SUPPLEMENTARY MATERIALS

www.sciencemag.org/content/344/6186/917/suppl/DC1
Materials and Methods
Figs. S1 to S13
Tables S1 to S8
References (*21*–*26*)

17 February 2014; accepted 11 April 2014
10.1126/science.1252328

Science
AAAS

Recurrent somatic mutations underlie corticotropin-independent Cushing's syndrome
Yusuke Sato *et al.*
Science **344**, 917 (2014);
DOI: 10.1126/science.1252328

Science (print ISSN 0036-8075; online ISSN 1095-9203) is published weekly, except the last week in December, by the American Association for the Advancement of Science, 1200 New York Avenue NW, Washington, DC 20005.

nature genetics

The genomic landscape of nasopharyngeal carcinoma

De-Chen Lin[1,2,12], Xuan Meng[1,3,12], Masaharu Hazawa[1], Yasunobu Nagata[4,5], Ana Maria Varela[1], Liang Xu[1], Yusuke Sato[4,5], Li-Zhen Liu[1], Ling-Wen Ding[1], Arjun Sharma[1], Boon Cher Goh[1,6], Soo Chin Lee[1,6], Bengt Fredrik Petersson[7], Feng Gang Yu[8], Paul Macary[9], Min Zin Oo[9], Chan Soh Ha[10], Henry Yang[1,13], Seishi Ogawa[4,5,13], Kwok Seng Loh[8,13] & H Phillip Koeffler[1,2,11,13]

Nasopharyngeal carcinoma (NPC) has extremely skewed ethnic and geographic distributions, is poorly understood at the genetic level and is in need of effective therapeutic approaches. Here we determined the mutational landscape of 128 cases with NPC using whole-exome and targeted deep sequencing, as well as SNP array analysis. These approaches revealed a distinct mutational signature and nine significantly mutated genes, many of which have not been implicated previously in NPC. Notably, integrated analysis showed enrichment of genetic lesions affecting several important cellular processes and pathways, including chromatin modification, ERBB-PI3K signaling and autophagy machinery. Further functional studies suggested the biological relevance of these lesions to the NPC malignant phenotype. In addition, we uncovered a number of new druggable candidates because of their genomic alterations. Together our study provides a molecular basis for a comprehensive understanding of, and exploring new therapies for, NPC.

NPC arises from the epithelial lining of the nasopharynx[1]. This neoplasm has remarkable ethnic and geographic distributions, with a particularly high prevalence in southern China, southeast Asia and northern Africa[2]. Genetic susceptibility[3,4], Epstein-Barr virus (EBV) infection[5] and chemical carcinogens[6,7] have been implicated in the pathogenesis of NPC. Several studies have identified multiple regions of chromosomal gains and losses in NPC[8–10]. Nevertheless, genomic abnormalities of this disease remain largely obscure, and no targeted therapy has been established. Therefore, a strong need exists to comprehensively characterize the genomic foundations of NPC to guide the development of new therapeutic regimens.

To address these issues, we first performed whole-exome sequencing (WES) of 56 NPC germline and tumor pairs (discovery cohort) and 5 NPC cell lines with a mean coverage of 86× (**Supplementary Tables 1a** and **2a**) and interrogated the somatic copy number variations (SCNVs) of 52 primary tumors with SNP array (of which 50 also had WES data). In addition, we performed transcriptome sequencing (RNA-seq) on four tumors from this cohort. We identified 1,577 non-silent somatic mutations affecting 1,413 genes (**Fig. 1a** and **Supplementary Table 3a**), revealing a relatively low mutational rate[11] (**Supplementary Fig. 1**) and wide mutational diversity. Subjects with NPC at more advanced clinical stages tended to have heavier mutational burdens, albeit not statistically significantly (**Fig. 1a**; $P = 0.059$). Validation of candidate mutations with Sanger sequencing showed that a true positive rate of 96.6% was achieved (**Supplementary Table 3a**). We analyzed intratumor clonal architecture using WES data and observed both biclonal and multiclonal signatures (**Supplementary Fig. 2**). Cross comparing WES with RNA-seq data from the same tumors revealed that 56% of the mutated genes had detectable transcripts (**Supplementary Table 4**). Investigators have previously noticed that tumors associated with human papillomavirus (for example, cervical and head and neck cancers) often show mutational spectrums caused by the DNA cytidine deaminase APOBEC3B[12–14]. To our surprise, although NPC is invariably associated with EBV infection (**Supplementary Table 2**), we discovered a distinct mutational signature in NPC, which is not contributed by APOBEC3B-induced mutagenesis (**Fig. 1b**, **Supplementary Fig. 3a,b** and **Supplementary Table 5**). Indeed, APOBEC3B expression was not significantly altered in this malignancy (**Supplementary Fig. 3c**).

Although the SNP array results revealed that copy number alterations were not common in NPC as compared with other types of solid tumors (**Fig. 1c**), this approach identified multiple recurrent SCNVs, with the most frequent deletion peak spanning *CDKN2A* on 9p21 (**Fig. 2**). We also observed additional SCNVs involving established cancer genes, including *CCND1*, *AKT2*, *MYC* and *TP53*. Notably, we identified that the gene encoding one component of the SWI/SNF complex, *ARID1A*, was frequently deleted in NPC (**Fig. 2**).

To determine the mutational events contributing to the NPC malignant phenotype (driver events), we first selected candidate driver

[1]Cancer Science Institute of Singapore, National University of Singapore, Singapore. [2]Division of Hematology/Oncology, Cedars-Sinai Medical Center, University of California, Los Angeles School of Medicine, Los Angeles, California, USA. [3]Department of Medicine, School of Medicine, National University of Singapore, Singapore. [4]Cancer Genomics Project, Graduate School of Medicine, The University of Tokyo, Tokyo, Japan. [5]Department of Pathology and Tumor Biology, Graduate School of Medicine, Kyoto University, Kyoto, Japan. [6]Department of Haematology-Oncology, National University Cancer Institute, Singapore. [7]Department of Pathology, National University Health System, Singapore. [8]Department of Otolaryngology, National University Hospital Singapore, Singapore. [9]Department of Immunology, National University of Singapore, Singapore. [10]Department of Microbiology, National University of Singapore, Singapore. [11]National University Cancer Institute, National University Hospital Singapore, Singapore. [12]These authors contributed equally to this work. [13]These authors jointly directed this work. Correspondence should be addressed to D.-C.L. (dchlin11@gmail.com).

Received 27 January; accepted 13 May; published online 22 June 2014; doi:10.1038/ng.3006

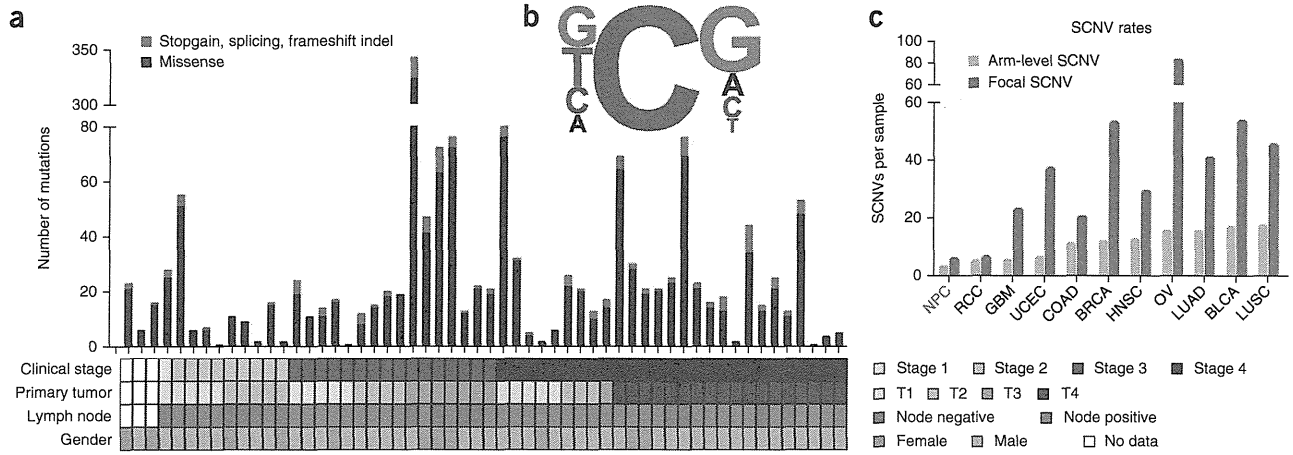

Figure 1 Somatic mutational rates and signatures and SCNVs in NPC. (**a**) The number of somatic mutations discovered from each paired NPC case subjected to WES and key clinical parameters (**Supplementary Table 2a**) clustered according to the clinical stage. Indel, insertion or deletion. (**b**) Trinucleotide contexts of somatic mutations occurring at cytosine nucleotides in NPC. The font size of the nucleotides at the 3′ and 5′ positions is proportional to their frequencies (**Supplementary Fig. 3b**). (**c**) Rates of arm-level and focal SCNVs (Online Methods) across different types of malignancies. Data regarding SCNVs of the following types were summarized from Zack *et al.*[50]: RCC, renal cell carcinoma; GBM, glioblastoma multiforme; UCEC, uterine cervix; COAD, colorectal adenocarcinoma; BRCA, breast; HNSC, head and neck squamous cell; OV, ovary; LUAD, lung adenocarcinoma; BLCA, bladder; LUSC, lung squamous cell.

genes from the discovery cohort on the basis of the following criteria: (i) genes with false discovery rates (FDR) <0.4, which was calculated by CHASM, a widely used algorithm to distinguish driver and passenger mutations[15–17]; (ii) genes with detectable transcripts in at least 50% of the tumors examined by RNA-seq (most passenger mutations have little or no expression[11]); or (iii) genes causally implicated in other solid tumors or involved in the canonical oncogenic pathways (Cancer Gene Census; see URLs). This process readily included well-studied cancer drivers such as *TP53*, *KRAS*, *ERBB2* and *PIK3CA* and excluded many common passenger mutations (for example, *TTN* and the genes encoding mucins, cytoskeletal dyneins and olfactory receptors), and we selected a total of 134 such candidate driver genes (**Supplementary Table 6**). We next deep sequenced all of the exons of these genes with an additional 61 NPC germline and tumor pairs and 5 nonpaired primary tumors (prevalence cohort, mean coverage 297×; **Supplementary Tables 1b** and **2b**). Combining the data from both cohorts, we discovered that 144 genes were mutated in at least two cases (**Supplementary Table 3**), with a number of hot-spot and double-hit mutations (**Fig. 2**), indicating their functional relevance. We identified nine significantly mutated genes through recalculating the FDR for all the mutations (FDR < 0.2; **Fig. 2**), and except for *TP53* (refs. 18,19) and *PIK3CA*[20,21], none of these genes has been implicated previously in NPC.

To interactively understand the genomic alterations in NPC, we performed unbiased Gene Ontology term enrichment and ingenuity pathway analysis of the mutational events[22,23] (Online Methods). The most noteworthy feature of the NPC genome is the presence of widespread alterations targeting the chromatin modification pathway ($P = 0.002$). We identified a total of 67 altered genes in 54 cases with NPC affecting multiple chromatin modification processes, indicating broad and heterogeneous insults in the epigenome of NPC (**Fig. 3a** and **Supplementary Table 7**). Notably, this category of alterations showed strong associations with both EBV burden (**Supplementary Table 8a**) and poor overall survival in univariate but not multivariate analysis (**Fig. 3c** and **Supplementary Table 8b,c**), indicating that dysregulation of chromatin modification might contribute to the aggressiveness of NPC. Notably, we also noticed a correlation between this cluster of mutations and a higher mutational burden, which may warrant further investigation (**Fig. 3b**).

The most frequently altered gene within this category was *ARID1A*, with 13 of 128 cases (10%) harboring deletions and/or mutations, followed by *MLL2* (6%), *BAP1* (4%), *MLL3* (4%) and *TET2* (4%). We found Knudson's double-hit tumor suppressor pattern (mutation and loss of heterozygosity) in several of these genes, including *ARID1A* (**Figs. 2** and **3a**). Because loss of *ARID1A* has also been observed in a variety of other cancer types[24], we sought to determine its cancer-related role in NPC cells. Depletion of wild-type endogenous ARID1A expression with short hairpin RNAs (shRNAs) led to markedly increased anchorage-independent colony formation, cell migration and xenograft growth (**Fig. 4a–d**). To validate the on-target effects of shRNA-mediated knockdown, we silenced ARID1A expression with an additional pool of small interfering RNAs (siRNAs) and observed similar results (**Supplementary Fig. 4a,b**). These effects were lost in HONE1 cells, which have undetectable ARID1A expression (**Supplementary Fig. 4c–f**), further confirming the specificity of the assays. The causes of compromised ARID1A expression in HONE1 cells appear to occur at the post-translational level, as we did not find deletions or possible hypermethylations in the *ARID1A* promoter region, and ARID1A mRNA levels in HONE1 cells were comparable to those in other cells (**Supplementary Fig. 4h–j**). Notably, inhibition of proteasome but not histone deacetylases markedly enhanced ARID1A protein levels in HONE1 cells (**Supplementary Fig. 4k**). We next ectopically expressed *ARID1A* and found suppression of both anchorage-independent colony formation and cell migration (**Fig. 4e–g**). ARID1A was previously reported to inhibit cell proliferation through regulating $p21^{WAF1}$ expression[25,26], which we confirmed in NPC cells (**Fig. 4d**). We found consistent upregulation of MYC (also called c-Myc) protein expression after depletion of ARID1A (**Fig. 4d** and **Supplementary Fig. 4g**), indicating that MYC might be a target of ARID1A in NPC cells.

BAP1 has a deubiquitinating function that belongs to the ubiquitin C-terminal hydrolase subfamily. Recently, BAP1 was shown to deubiquitinate histone H2A, which is vital for the function of the Polycomb group of transcriptional repressors[27]. *BAP1* somatic mutations

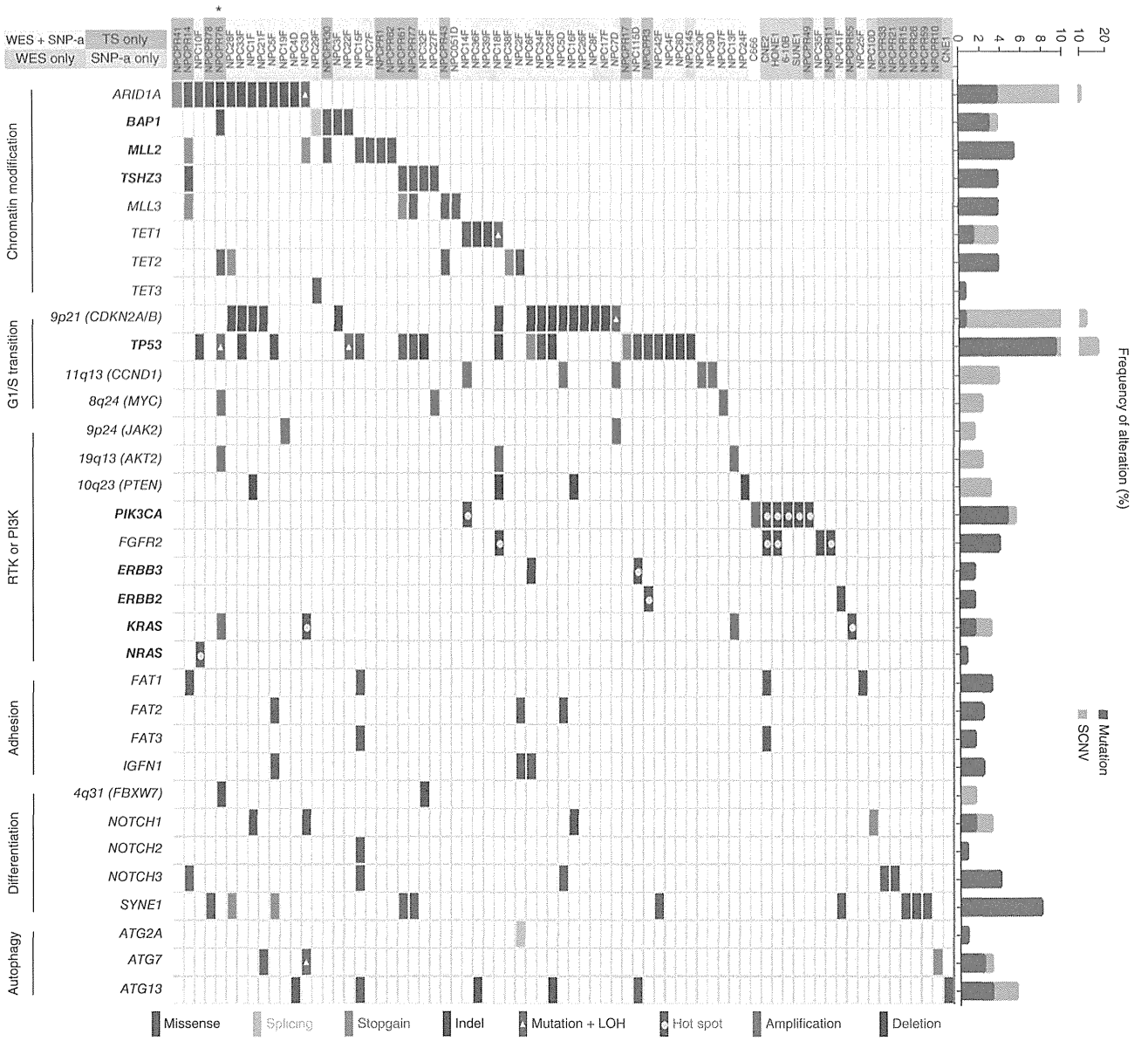

Figure 2 Integrated analysis of genetic alterations in NPC. Data matrix showing frequent SCNVs, significantly mutated genes (bold; Benjamini-Hochberg FDR < 0.2 calculated with CHASM) and their associated pathway or family mutations discovered in cases with NPC analyzed by WES, targeted deep sequencing (TS) or SNP array (SNP-a). The frequencies of the alterations are plotted on the right. The colors and shapes denoting different types of somatic events are also applied in **Figure 5a**. Columns, examined cases; rows, genes; hot spot, identical mutations have been registered in COSMIC (see URLs); LOH, loss of heterozygosity. The asterisk indicates that this tumor was also subjected to SNP array profiling. *PIK3CA* amplification in C666 cells has been previously described[20].

have been observed in several types of tumors, including renal cell carcinoma[28–30], uveal melanoma[31] and cholangiocarcinoma[32,33]. As *BAP1* was significantly mutated and deleted in our study, we examined its functional role in NPC cells. Ectopic expression of wild-type BAP1 suppressed colony growth in soft agar (**Fig. 4h,i**). Collectively, these genetic alterations and biological results strongly suggest that both *ARID1A* and *BAP1* encode tumor suppressors that are frequently lost in NPC.

Another prominently altered pathway in NPC is the ERBB-PI3K signaling pathway ($P = 2.04 \times 10^{-4}$), with the majority of these somatic events being mutually exclusive (**Fig. 5a**). *PIK3CA* was the most frequently dysregulated oncogene, activated by both well-characterized hot-spot mutations (for example, those encoding p.His1047Arg and p.Glu545Lys) and amplification (6% in total). Mutations in *ERBB2* or *ERBB3* were present in four tumors, with two of these mutations having been reported previously in other cancers, suggesting their functional relevance. Additional lesions included *KRAS* amplification and Gly12 mutation, *AKT2* amplification and *PTEN* deletion. Notably, subjects with alterations in this pathway tended to have shorter survival time than subjects without such mutations in univariate but not multivariate analysis (**Fig. 5b** and **Supplementary Table 8b,c**). This cluster of subjects also presented more advanced clinical stage ($P = 0.036$; **Supplementary Table 9a**), suggesting that ERBB-PI3K pathway activation by genetic alterations exacerbated NPC malignancy. Because

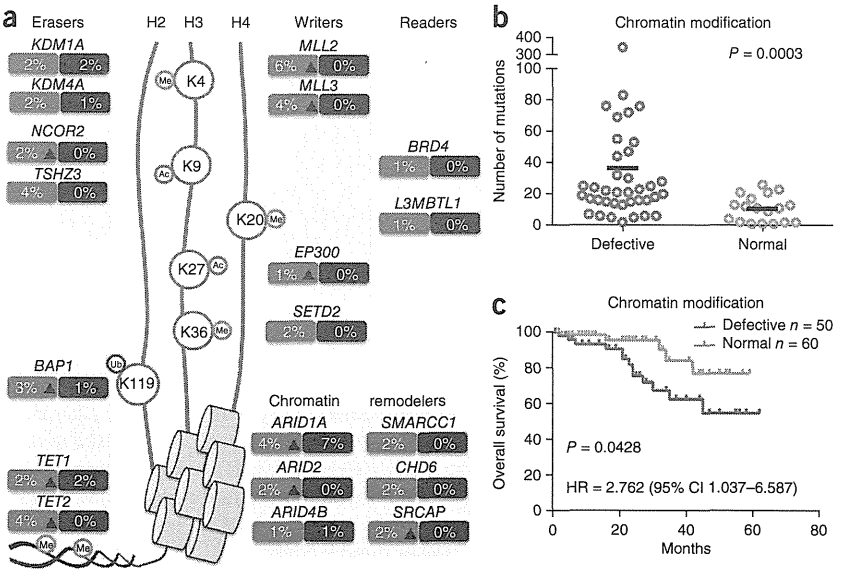

Figure 3 Chromatin modification processes dysregulated by genomic alterations in NPC. (**a**) Frequently altered genes involved in chromatin modification processes, with each molecule positioned in parallel with its modification sites in different histones or DNA (*TET1* and *TET2*). The entire gene list is shown in **Supplementary Table 7**. Somatic mutations are marked in gray, and deletions are in blue. A triangle indicates that truncating mutations (including frameshift indel, splicing site and stopgain) occurred. K, lysine; Ac, acetylation; Me, methylation; Ub, ubiquitination. (**b**,**c**) Significant correlations between dysregulation of chromatin modification and total number of somatic mutations (**b**) and overall survival probability (**c**). Mann-Whitney test (**b**) and log-rank test (**c**) were used to calculate statistical significance. Horizontal bars, mean value; HR, hazard ratio.

this oncogenic pathway contains many actionable kinases, we correlated this category of genomic events with targeted therapeutic approaches that have either been approved for clinical use or are under evaluation in clinical trials (**Fig. 5a**). Our results reveal that a number of previously unrecognized candidate therapeutic targets exist in NPC that need further investigation.

Besides prevailing somatic events targeting chromatin modification and the ERBB-PI3K pathway, the autophagy machinery was shown to malfunction by mutations and deletions of three critical autophagic genes, namely *ATG2A* (1%), *ATG7* (2%) and *ATG13* (5%). Although not attaining statistical significance in an enrichment analysis, to our knowledge, these results reveal for the first time somatic mutations directly targeting autophagy machinery factors in human cancers. By capturing, digesting and recycling damaged proteins and organelles,

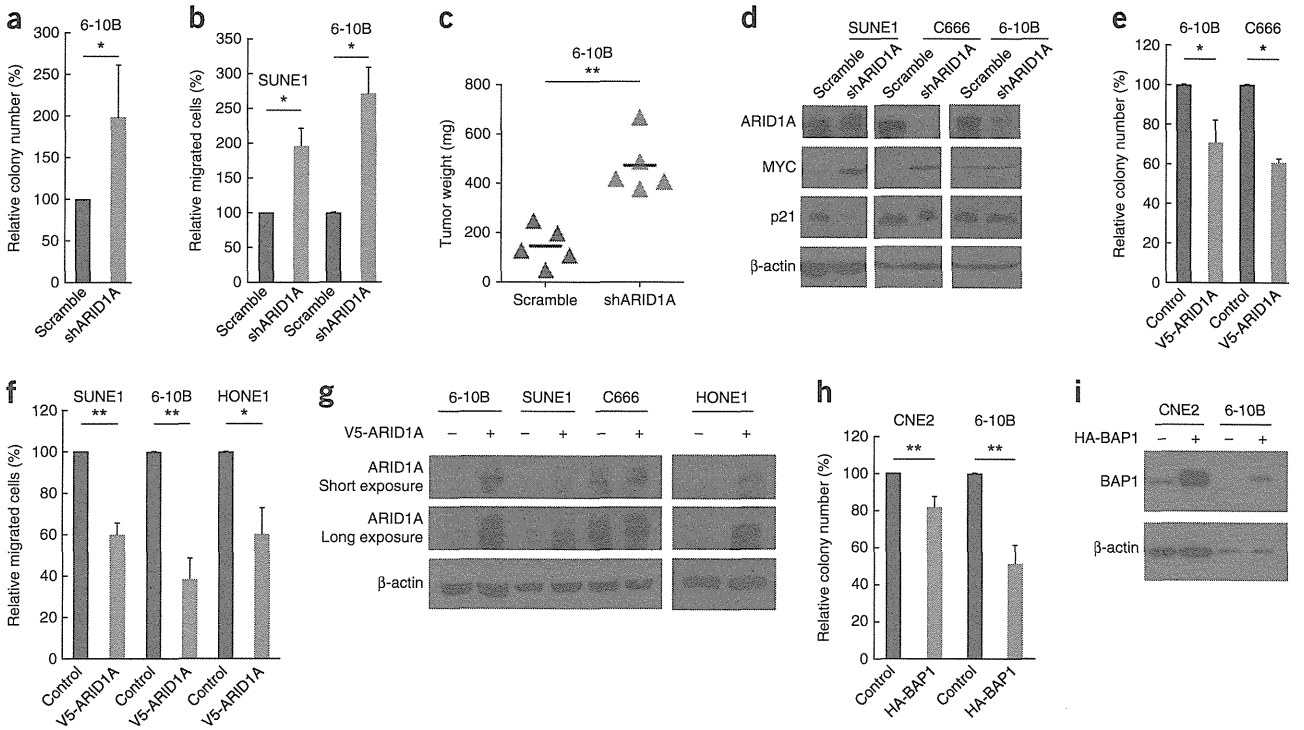

Figure 4 Identification of ARID1A and BAP1 as NPC tumor suppressors. (**a**–**d**) NPC cells stably expressing either negative control shRNA (Scramble) or pooled shRNAs targeting ARID1A (shARID1A) were subjected to anchorage-independent colony formation assay (**a**), migration assay (**b**), xenograft growth assay (horizontal lines, mean values) and western blot (WB) assay with the indicated antibodies (**d**). (**e**–**g**) NPC cells either with or without exogenously expressing ARID1A were examined by anchorage-independent colony formation assay (**e**), migration assay (**f**) and WB assay with the indicated antibodies (**g**). (**h**,**i**) NPC cells either with or without exogenously expressing BAP1 were examined by anchorage-independent colony formation assay (**h**) and WB assay with indicated antibodies (**i**). β-actin was examined as a loading control. The data shown in **a**, **b**, **e**, **f** and **h** represent the mean ± s.d.; $n = 3$ for **a**, **b**, **e** and **f**; $n = 4$ for **h**. $^{*}P < 0.05$, $^{**}P < 0.01$. Student's *t*-test was used to calculate statistical significance in **a**–**c**, **e**, **f** and **h**; the blots shown in **d**, **g** and **i** are representative of three total blots run.

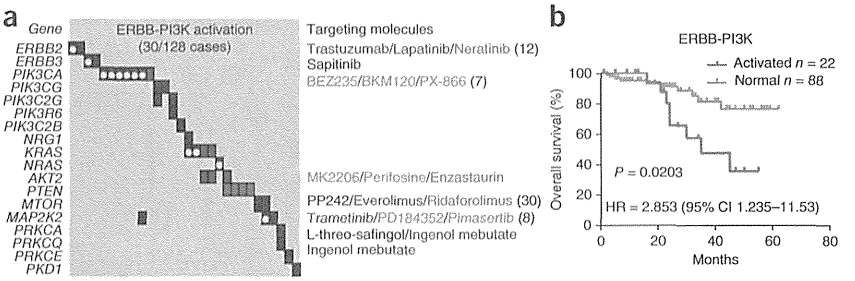

Figure 5 Actionable genomic lesions in NPC. (**a**) Data matrix showing alterations of genes involved in the ERBB-PI3K signaling pathway and their related targeting molecules. Considering space limitations, the numbers of targeting agents available for each protein are shown in parentheses. Drugs currently in phase 2 clinical trials are marked in blue, those in phase 3 are in purple, and FDA-approved drugs are in brown (see URLs). (**b**) Kaplan-Meier survival curves of NPC subjects either with or without genetic lesions in the ERBB-PI3K signaling pathway. Log-rank test was used to calculate statistical significance.

autophagy is a vital process to maintain cellular homeostasis. The role of autophagy in cancer is intricate and context dependent. During the initiation of malignancy, autophagy is tumor suppressive by reducing chronic tissue damage and oxidative stress (reviewed in ref. 34). The frequent inactivation of autophagic factors observed in the current study also suggests that autophagy might prevent the development of NPC tumors. Conversely, in advanced tumors, autophagy protects cancer cells from chemotherapy-triggered stress and apoptosis through induction of either dormancy or quiescence, and thus inhibition of autophagy becomes therapeutically advantageous[35–37]. Indeed, combining chemotherapies with either an autophagy-blocking agent or genetic ablation of autophagy has demonstrated preclinical success[38–40] and is currently under evaluation in clinical trials (see URLs). Notably, we also found that combinational treatment with cisplatin and chloroquine (an autophagy-blocking agent) synergistically impaired the viability of NPC cells *in vitro* (**Supplementary Fig. 5a**). Our data suggest that a substantial portion of NPC tumors (8%) were intrinsically defective in the autophagy pathway and thus might respond sensitively to chemotherapeutic regimens. The identification of such susceptible patients through genomic approaches before chemotherapeutic treatments might offer particular clinical benefits.

We found additional noteworthy pathways and gene families that were frequently targeted by genetic abnormalities in NPC. The epithelial cell differentiation program was dysregulated mostly by *SYNE1* mutations (8%) and mutations and deletions of *NOTCH* family genes (7% in total; **Fig. 2**), which have also been noticed in lung[41] and head and neck[42,43] cancers. The SYNE1 protein operates upstream of NOTCH1 and promotes NOTCH1-dependent epidermal differentiation[44]. G1/S cell cycle transition was affected in 28% of NPCs, with most of the alterations occurring in *CDKN2A* and *TP53*. This process was further targeted by amplifications at the *CCND1* and *MYC* locus (**Fig. 2**). We also noticed frequent but not statistically significant mutations affecting the FAT gene family, including *FAT1* (3%), *FAT2* (2%) and *FAT3* (2%). Very recently, loss-of-function mutations of *FAT1* have been reported in glioblastoma, colon and head and neck cancers[45]. We also found that *FAT1* was recurrently disrupted in esophageal tumors through truncating mutations and deletions[46]. However, the precise role of *FAT1* in cancer is still inconclusive and appears to be tissue specific[47,48]. Unlike the widespread truncating mutations reported in other types of malignancies, all of the mutations observed in NPC tumors were missense and were predicted by PolyPhen-2 (ref. 49) to not be deleterious. Moreover, neither silencing of endogenous FAT1 expression with siRNA nor ectopic expression of FAT1 cDNA affected the proliferation of NPC cells (**Supplementary Fig. 5b,c**), indicating that the biological relevance of *FAT* mutations in NPC might be complex and will require further investigation.

In summary, we performed integrated analysis of the genomic landscape of 128 cases with NPC and, together with *ARID1A* and *BAP1*, identified a number of new driver genes with statistical and/or biological evidence. We also highlighted pathway derangements involving chromatin modification, ERBB-PI3K signaling and autophagy machinery, all of which offer potential avenues for treatments to address this fatal disease. These data together provide an enhanced road map for the study of the molecular basis underlying this deadly malignancy.

URLs. dbSNP, http://www.ncbi.nlm.nih.gov/projects/SNP/; 1000 Genomes Project, http://www.1000genomes.org/; CNAG/AsCNAR, http://www.genome.umin.jp/; COSMIC, http://cancer.sanger.ac.uk/cancergenome/projects/cosmic/; Cancer Gene Census, http://cancer.sanger.ac.uk/cancergenome/projects/census/; clinical trials database, http://clinicaltrials.gov/; drugs approved by US Food and Drug Administration (FDA), http://www.fda.gov/; Picard, http://picard.sourceforge.net/; Ingenuity Pathway Analysis (IPA), http://www.ingenuity.com/products/ipa.

METHODS

Methods and any associated references are available in the online version of the paper.

Accession codes. Digital sequencing and SNP array files have been deposited into Sequence Read Archive (SRP035573) and Gene Expression Omnibus (GSE57100), respectively.

Note: Any Supplementary Information and Source Data files are available in the online version of the paper.

ACKNOWLEDGMENTS

We thank M.-S. Zeng (Sun Yat-sen University Cancer Center), T. Chan (Memorial Sloan-Kettering Cancer Center), Z.J. Zang (National Cancer Centre Singapore) and P. Tan for generously sharing materials as well as relevant facilities. This work is supported by US National Institutes of Health grant R01CA026038-35 (H.P.K.), the National Research Foundation Singapore and the Singapore Ministry of Education under the Research Centres of Excellence initiative (H.P.K.) and the Singapore Ministry of Health's National Medical Research Council under its Singapore Translational Research (STaR) Investigator Award to H.P.K. This work is also supported by The Terry Fox Foundation International Run Program through funds raised by the Terry Fox Singapore Run to the National University Cancer Institute, Singapore (NCIS).

AUTHOR CONTRIBUTIONS

D.-C.L. and H.P.K. designed the study and wrote the manuscript. D.-C.L., X.M., M.H., Y.N., Y.S., A.M.V., L.X., L.-W.D. and A.S. performed experiments. C.S.H., B.F.P., B.C.G., S.C.L., F.G.Y. and K.S.L. coordinated sample collection and processing. D.-C.L., Y.N., Y.S., L.-Z.L., H.Y. and S.O. performed bioinformatical analysis. D.-C.L., X.M., Y.N., P.M., M.Z.O., B.C.G., S.C.L., F.G.Y., H.Y., S.O., K.S.L. and H.P.K. analyzed and discussed the data.

COMPETING FINANCIAL INTERESTS

The authors declare no competing financial interests.

1. Wei, W.I. & Sham, J.S. Nasopharyngeal carcinoma. *Lancet* **365**, 2041–2054 (2005).
2. Yu, M.C. & Yuan, J.M. Epidemiology of nasopharyngeal carcinoma. *Semin. Cancer Biol.* **12**, 421–429 (2002).
3. Bei, J.X. *et al.* A genome-wide association study of nasopharyngeal carcinoma identifies three new susceptibility loci. *Nat. Genet.* **42**, 599–603 (2010).
4. Feng, B.J. *et al.* Genome-wide scan for familial nasopharyngeal carcinoma reveals evidence of linkage to chromosome 4. *Nat. Genet.* **31**, 395–399 (2002).
5. Andersson-Anvret, M., Forsby, N., Klein, G. & Henle, W. Relationship between the Epstein-Barr virus and undifferentiated nasopharyngeal carcinoma: correlated nucleic acid hybridization and histopathological examination. *Int. J. Cancer* **20**, 486–494 (1977).
6. Yu, M.C., Mo, C.C., Chong, W.X., Yeh, F.S. & Henderson, B.E. Preserved foods and nasopharyngeal carcinoma: a case-control study in Guangxi, China. *Cancer Res.* **48**, 1954–1959 (1988).
7. Ward, M.H. *et al.* Dietary exposure to nitrite and nitrosamines and risk of nasopharyngeal carcinoma in Taiwan. *Int. J. Cancer* **86**, 603–609 (2000).
8. Chan, A.S. *et al.* High frequency of chromosome 3p deletion in histologically normal nasopharyngeal epithelia from southern Chinese. *Cancer Res.* **60**, 5365–5370 (2000).
9. Sheu, J.J. *et al.* Chromosome 3p12.3-p14.2 and 3q26.2-q26.32 are genomic markers for prognosis of advanced nasopharyngeal carcinoma. *Cancer Epidemiol. Biomarkers Prev.* **18**, 2709–2716 (2009).
10. Hu, C. *et al.* A global view of the oncogenic landscape in nasopharyngeal carcinoma: an integrated analysis at the genetic and expression levels. *PLoS ONE* **7**, e41055 (2012).
11. Lawrence, M.S. *et al.* Mutational heterogeneity in cancer and the search for new cancer-associated genes. *Nature* **499**, 214–218 (2013).
12. Burns, M.B., Temiz, N.A. & Harris, R.S. Evidence for APOBEC3B mutagenesis in multiple human cancers. *Nat. Genet.* **45**, 977–983 (2013).
13. Roberts, S.A. *et al.* An APOBEC cytidine deaminase mutagenesis pattern is widespread in human cancers. *Nat. Genet.* **45**, 970–976 (2013).
14. Burns, M.B. *et al.* APOBEC3B is an enzymatic source of mutation in breast cancer. *Nature* **494**, 366–370 (2013).
15. Carter, H. *et al.* Cancer-specific high-throughput annotation of somatic mutations: computational prediction of driver missense mutations. *Cancer Res.* **69**, 6660–6667 (2009).
16. Carter, H., Samayoa, J., Hruban, R.H. & Karchin, R. Prioritization of driver mutations in pancreatic cancer using cancer-specific high-throughput annotation of somatic mutations (CHASM). *Cancer Biol. Ther.* **10**, 582–587 (2010).
17. Wong, W.C. *et al.* CHASM and SNVBox: toolkit for detecting biologically important single nucleotide mutations in cancer. *Bioinformatics* **27**, 2147–2148 (2011).
18. Sun, Y. *et al.* An infrequent point mutation of the p53 gene in human nasopharyngeal carcinoma. *Proc. Natl. Acad. Sci. USA* **89**, 6516–6520 (1992).
19. Chakrani, F. *et al.* Mutations clustered in exon 5 of the p53 gene in primary nasopharyngeal carcinomas from southeastern Asia. *Int. J. Cancer* **61**, 316–320 (1995).
20. Or, Y.Y., Hui, A.B., To, K.F., Lam, C.N. & Lo, K.W. *PIK3CA* mutations in nasopharyngeal carcinoma. *Int. J. Cancer* **118**, 1065–1067 (2006).
21. Chou, C.C., Chou, M.J. & Tzen, C.Y. *PIK3CA* mutation occurs in nasopharyngeal carcinoma but does not significantly influence the disease-specific survival. *Med. Oncol.* **26**, 322–326 (2009).
22. Eden, E., Lipson, D., Yogev, S. & Yakhini, Z. Discovering motifs in ranked lists of DNA sequences. *PLoS Comput. Biol.* **3**, e39 (2007).
23. Eden, E., Navon, R., Steinfeld, I., Lipson, D. & Yakhini, Z. GOrilla: a tool for discovery and visualization of enriched GO terms in ranked gene lists. *BMC Bioinformatics* **10**, 48 (2009).
24. Wu, J.N. & Roberts, C.W. *ARID1A* mutations in cancer: another epigenetic tumor suppressor? *Cancer Discov.* **3**, 35–43 (2013).
25. Guan, B., Gao, M., Wu, C.H., Wang, T.L. & Shih Ie, M. Functional analysis of in-frame indel *ARID1A* mutations reveals new regulatory mechanisms of its tumor suppressor functions. *Neoplasia* **14**, 986–993 (2012).
26. Guan, B., Wang, T.L. & Shih Ie, M. *ARID1A*, a factor that promotes formation of SWI/SNF-mediated chromatin remodeling, is a tumor suppressor in gynecologic cancers. *Cancer Res.* **71**, 6718–6727 (2011).
27. Scheuermann, J.C. *et al.* Histone H2A deubiquitinase activity of the Polycomb repressive complex PR-DUB. *Nature* **465**, 243–247 (2010).
28. Cancer Genome Atlas Research Network. Comprehensive molecular characterization of clear cell renal cell carcinoma. *Nature* **499**, 43–49 (2013).
29. Peña-Llopis, S. *et al.* BAP1 loss defines a new class of renal cell carcinoma. *Nat. Genet.* **44**, 751–759 (2012).
30. Sato, Y. *et al.* Integrated molecular analysis of clear-cell renal cell carcinoma. *Nat. Genet.* **45**, 860–867 (2013).
31. Harbour, J.W. *et al.* Frequent mutation of *BAP1* in metastasizing uveal melanomas. *Science* **330**, 1410–1413 (2010).
32. Chan-On, W. *et al.* Exome sequencing identifies distinct mutational patterns in liver fluke–related and non-infection–related bile duct cancers. *Nat. Genet.* **45**, 1474–1478 (2013).
33. Jiao, Y. *et al.* Exome sequencing identifies frequent inactivating mutations in *BAP1*, *ARID1A* and *PBRM1* in intrahepatic cholangiocarcinomas. *Nat. Genet.* **45**, 1470–1473 (2013).
34. White, E. Deconvoluting the context-dependent role for autophagy in cancer. *Nat. Rev. Cancer* **12**, 401–410 (2012).
35. Amaravadi, R.K. *et al.* Principles and current strategies for targeting autophagy for cancer treatment. *Clin. Cancer Res.* **17**, 654–666 (2011).
36. Garber, K. Inducing indigestion: companies embrace autophagy inhibitors. *J. Natl. Cancer Inst.* **103**, 708–710 (2011).
37. White, E. & DiPaola, R.S. The double-edged sword of autophagy modulation in cancer. *Clin. Cancer Res.* **15**, 5308–5316 (2009).
38. Amaravadi, R.K. *et al.* Autophagy inhibition enhances therapy-induced apoptosis in a Myc-induced model of lymphoma. *J. Clin. Invest.* **117**, 326–336 (2007).
39. Bellodi, C. *et al.* Targeting autophagy potentiates tyrosine kinase inhibitor–induced cell death in Philadelphia chromosome–positive cells, including primary CML stem cells. *J. Clin. Invest.* **119**, 1109–1123 (2009).
40. Sheen, J.H., Zoncu, R., Kim, D. & Sabatini, D.M. Defective regulation of autophagy upon leucine deprivation reveals a targetable liability of human melanoma cells *in vitro* and *in vivo*. *Cancer Cell* **19**, 613–628 (2011).
41. Cancer Genome Atlas Research Network. Comprehensive genomic characterization of squamous cell lung cancers. *Nature* **489**, 519–525 (2012).
42. Agrawal, N. *et al.* Exome sequencing of head and neck squamous cell carcinoma reveals inactivating mutations in *NOTCH1*. *Science* **333**, 1154–1157 (2011).
43. Stransky, N. *et al.* The mutational landscape of head and neck squamous cell carcinoma. *Science* **333**, 1157–1160 (2011).
44. Williams, S.E., Beronja, S., Pasolli, H.A. & Fuchs, E. Asymmetric cell divisions promote Notch-dependent epidermal differentiation. *Nature* **470**, 353–358 (2011).
45. Morris, L.G. *et al.* Recurrent somatic mutation of *FAT1* in multiple human cancers leads to aberrant Wnt activation. *Nat. Genet.* **45**, 253–261 (2013).
46. Lin, D.C. *et al.* Genomic and molecular characterization of esophageal squamous cell carcinoma. *Nat. Genet.* **46**, 467–473 (2014).
47. de Bock, C.E. *et al.* The Fat1 cadherin is overexpressed and an independent prognostic factor for survival in paired diagnosis-relapse samples of precursor B-cell acute lymphoblastic leukemia. *Leukemia* **26**, 918–926 (2012).
48. Dikshit, B. *et al.* FAT1 acts as an upstream regulator of oncogenic and inflammatory pathways, via PDCD4, in glioma cells. *Oncogene* **32**, 3798–3808 (2013).
49. Adzhubei, I.A. *et al.* A method and server for predicting damaging missense mutations. *Nat. Methods* **7**, 248–249 (2010).
50. Zack, T.I. *et al.* Pan-cancer patterns of somatic copy number alteration. *Nat. Genet.* **45**, 1134–1140 (2013).

ONLINE METHODS

Sample collection and assessment. All cases with NPC were diagnosed in Singapore, and biopsy tissues and paired peripheral blood samples were collected from National University Hospital Singapore. All biopsy tissues were residual specimens collected after diagnosis, and no patient received preoperative treatments. To assess the cellularity of malignant cells and infiltration of lymphocytes by pathological review, multiple (if applicable) slides of each biopsy sample were either stained with hematoxylin and eosin and/or immunohistochemically reacted with antibodies (AE1/AE3, 1:100, DAKO) against cytokeratins (**Supplementary Table 2a,b**). To further examine the tumor cellularity, we analyzed the heterogeneity of all tumors by calculating the variant allele frequency for somatic mutations of dominant clones (**Supplementary Table 2a,b**)[51]. Concentrations of circulating EBV DNA in the peripheral blood of each case are provided in **Supplementary Table 2a,b**. All patients signed individual consent forms for the sample collection and molecular analysis. This study has been approved by the Institutional Review Board of National University Hospital Singapore.

WES, TS and RNA-seq. For WES, exome capture was performed using the SureSelect Human All Exon 50M kit (Agilent Technologies) according to the manufacturer's protocols. For TS, a customized DNA enrichment kit (SureSelect, Agilent Technologies) was designed and used to capture all the exons from 134 genes (**Supplementary Table 6**). For RNA-seq, libraries were generated using the TruSeq RNA Sample Preparation kit (Illumina) as described previously[30]. Captured nucleotides were subjected to massively parallel sequencing using HiSeq2000 platform (Illumina) with 75- to 100-bp paired-end reads.

Detection of somatic mutations. Previously described in-house mathematic algorithms[30,52–54] were employed to detect somatic nucleotide variations from WES and TS. Briefly, massively parallel sequencing reads were first aligned to hg19 using Burrows-Wheeler Aligner (V 0.5.8) with default parameters. PCR duplicates were removed by Picard (see URLs). Next, the statistical significance of each candidate single nucleotide variant (SNV) was calculated by enumerating the number of reference bases and candidate SNVs with Fisher's Exact test, and those with $P < 0.01$ were analyzed further. Finally, the following SNVs were eliminated: (i) read depth fewer than ten in either the tumor or germline; (ii) SNP identified using sequencing data from paired normal DNA; or (iii) variants registered in either dbSNP131 or the 1000 Genomes project.

To detect probable somatic mutations of five NPC cell lines and five non-paired tumors that do not have matched germline DNA, besides all the aforementioned criteria applied, we further removed copy number–neutral variants with allele frequency between 45% and 55% unless they were registered in the COSMIC.

SNP array profiling. Genome-wide SCNV analysis (SNP array) was performed using the Affymetrix GeneChip Human Mapping 250K NspI Array according to the manufacturer's protocol. SNP array data were analyzed to determine total and allele-specific SCNVs with CNAG/AsCNAR algorithms as previously described[55,56]. Focal SCNVs (shorter than the chromosome arm) and arm-level SCNVs (chromosome-arm length or longer) were determined as previously defined[50].

Analysis of significantly altered pathways. Enriched gene sets reflecting biological processes annotated by Gene Ontology were calculated using the WEB-based GEne SeT AnaLysis Toolkit (WebGestalt)[23]. In parallel, additional enriched signaling pathways were identified using IPA (Ingenuity Systems). Multiple test–corrected *P* values were calculated when a hypergeometric distribution was applied[57,58]. To be more stringent, we assumed that all tumors had the same mutational rate as tumors with a defective chromatin modification pathway when calculating the enrichment of this process, considering that the tumors with mutations targeting chromatin modification had a heavier mutational burden compared to those tumors without such mutations (**Fig. 3b**).

Cell culture and chemicals. NPC cells and 293T cells were grown in RPMI-1640 and DMEM with 10% fetal calf serum, respectively. The cell lines CNE1, CNE2, SUNE1, 6-10B and HONE1 were generously provided by M.-S. Zeng (Sun Yat-sen University Cancer Center). All cell lines were recently tested for the absence of mycoplasma. Vorinostat (SML0061) and chloroquine (C6628) were purchased from Sigma-Aldrich.

WB assay. The whole-cell lysates were prepared with extraction buffer (50 mM Tris-HCl, pH 7.4, 150 mM NaCl and 0.5% Nonidet P-40) supplemented with complete protease and phosphatase inhibitor cocktail (Roche). The procedures for standard WB were performed as described previously[59]. The antibody specific for $p21^{WAF1}$(2947, 1:1,000) was purchased from Cell Signaling Technology; ARID1A (04-080, 1:1,000) was purchased from Millipore; BAP1 (SC-28383, 1:500), α-tubulin (SC-8035, 1:250) and MYC (SC-788, 1:250) were purchased from Santa Cruz Biotechnology; and FAT1 (HPA023882, 1:250) and β-actin (A5316, 1:5,000) were purchased from Sigma-Aldrich. The intensity of protein expression was quantified with ImageJ software.

Short-term cell proliferation assays. 6-10B and HONE1 cells were seeded on the 96-well plates at optimized confluence in triplicate and were grown for a total of 4 d. To quantify the number of cells, 3-(4, 5-dimethylthiazol–2-yl)-2, 5-diphenyltetrazolium bromide (MTT) incorporation was performed as described previously[60].

Migration assay. NPC cells were seeded onto transwell inserts (Corning, 3422) in 24-well plates and incubated for 48 h. The inserts were washed with PBS, and non-migrating cells were wiped off from the top side. Migrated cells were fixed with 4% paraformaldehyde and stained with 4′,6-diamidino-2-phenylindole (DAPI), and nuclei were counted.

Anchorage-independent colony formation assay. NPC cells premixed with 0.5% agar in medium were plated on top of 0.65% agar in 12-well plates in triplicate. Cells were grown for 2–3 weeks to form colonies and were stained with 0.01% crystal violet and counted.

cDNA vectors, shRNA vectors and siRNAs. Both the human ARID1A (Addgene plasmid number 39478) and human BAP1 (Addgene plasmid number 22539) cDNA expression vectors were obtained from Addgene under the terms defined by their Material Transfer Agreement, and cells constitutively expressing Tet repressor were generated to ectopically express ARID1A[26,61]. The ORF of the human FAT1 transcript was generously provided by T. Chan (Memorial Sloan-Kettering Cancer Center). The FAT1 ORF was subcloned into the lentiviral-based expression vector SHC003 (Sigma-Aldrich) using NheI and FseI cloning sites (the cloning primers used are shown in **Supplementary Table 10a**). SHC003-Turbo-GFP served as a control (Sigma-Aldrich). Lentiviral-based pooled shRNAs (**Supplementary Table 10b**) against human ARID1A were generously provided by Z.J. Zang (National Cancer Centre Singapore) and used as described before[62]. Lentiviral-based scramble shRNA was used as a negative control (Santa Cruz, sc-108060; **Supplementary Table 10b**). Pooled siRNAs targeting human ARID1A (M-017263-01; **Supplementary Table 10c**) and FAT1 (M-010513-02; **Supplementary Table 10d**) and scramble siRNA (D-001210-01; **Supplementary Table 10c,d**) were purchased from Thermo Scientific.

Transfections, viral particle production and infection. DNA and siRNA transfections were performed using Lipofectamine 2000 and Lipofectamine RNAiMAX (Life Technologies), respectively. Lentiviral particles were produced with the MISSION Lentiviral Packaging System (Sigma-Aldrich). NPC cells were transduced with the lentiviral particles in the presence of 8 μg/ml Polybrene (Sigma-Aldrich) for 48 h.

Methylation-specific PCR assay. Genomic DNA of HONE1 cells was modified by bisulfite using the EpiTect Bisulfite Kit (59104, Qiagen). Potential CpG islands within the *ARID1A* promoter region were computationally predicted by MethPrimer[63]. Primers specific for the unmethylated (U) and methylated (M) sequences were designed by MethPrimer[63] and are listed in **Supplementary Table 10e**.

Real-time RT-PCR assay. The real-time RT-PCR was performed using KAPA SYBR qPCR kits (KAPA Biosystems) in a 7500 real-time PCR system (Applied

Biosystems) according to the manufacturer's instructions. The relative mRNA expression level of ARID1A was calculated using GAPDH as a loading control. The primers used are listed in **Supplementary Table 10a**.

Xenograft growth. Male nonobese diabetic severe combined immunodeficient (NOD-SCID) mice (5–6 weeks of age) were purchased from the Cancer Science Institute of Singapore. Three million NPC cells were mixed with 100 µl of Matrigel (BD Biosciences) and injected subcutaneously in the upper flanks of mice, which were randomly allocated. After 4–6 weeks, mice were euthanized to weigh and analyze the dissected tumors. In these experiments, no statistical methods were employed to determine the sample size, and no blinding of investigators was performed. The mouse study was performed in compliance with ethical regulations of the Institutional Animal Care and Use Committee (IACUC) of the National University of Singapore.

Statistical analyses. The FDR q values for mutated genes were calculated using CHASM with default parameters[16,17,64]. Two-tailed Student's t-test was used in the statistical analysis of the following assays after verification of the assumptions (for example, normality): short-term cell proliferation assay, xenograft growth assay, migration assay and anchorage-independent colony formation assay. Overall survival probability was analyzed using either log-rank test (univariate analysis) or a Cox proportional hazards model (multivariate analysis).

51. Govindan, R. *et al.* Genomic landscape of non-small cell lung cancer in smokers and never-smokers. *Cell* **150**, 1121–1134 (2012).
52. Sakaguchi, H. *et al.* Exome sequencing identifies secondary mutations of *SETBP1* and *JAK3* in juvenile myelomonocytic leukemia. *Nat. Genet.* **45**, 937–941 (2013).
53. Yoshida, K. *et al.* Frequent pathway mutations of splicing machinery in myelodysplasia. *Nature* **478**, 64–69 (2011).
54. Yoshida, K. *et al.* The landscape of somatic mutations in Down syndrome–related myeloid disorders. *Nat. Genet.* **45**, 1293–1299 (2013).
55. Nannya, Y. *et al.* A robust algorithm for copy number detection using high-density oligonucleotide single nucleotide polymorphism genotyping arrays. *Cancer Res.* **65**, 6071–6079 (2005).
56. Yamamoto, G. *et al.* Highly sensitive method for genomewide detection of allelic composition in nonpaired, primary tumor specimens by use of Affymetrix single-nucleotide-polymorphism genotyping microarrays. *Am. J. Hum. Genet.* **81**, 114–126 (2007).
57. Zhang, B., Kirov, S. & Snoddy, J. WebGestalt: an integrated system for exploring gene sets in various biological contexts. *Nucleic Acids Res.* **33**, W741–W748 (2005).
58. Wang, J., Duncan, D., Shi, Z. & Zhang, B. WEB-based GEne SeT AnaLysis Toolkit (WebGestalt): update 2013. *Nucleic Acids Res.* **41**, W77–W83 (2013).
59. Lin, D.C. *et al.* Adaptor protein Lnk binds to and inhibits normal and leukemic FLT3. *Blood* **120**, 3310–3317 (2012).
60. Lin, D.C. *et al.* Genomic and functional characterizations of phosphodiesterase subtype 4D in human cancers. *Proc. Natl. Acad. Sci. USA* **110**, 6109–6114 (2013).
61. Sowa, M.E., Bennett, E.J., Gygi, S.P. & Harper, J.W. Defining the human deubiquitinating enzyme interaction landscape. *Cell* **138**, 389–403 (2009).
62. Zang, Z.J. *et al.* Exome sequencing of gastric adenocarcinoma identifies recurrent somatic mutations in cell adhesion and chromatin remodeling genes. *Nat. Genet.* **44**, 570–574 (2012).
63. Li, L.C. & Dahiya, R. MethPrimer: designing primers for methylation PCRs. *Bioinformatics* **18**, 1427–1431 (2002).
64. Douville, C. *et al.* CRAVAT: cancer-related analysis of variants toolkit. *Bioinformatics* **29**, 647–648 (2013).

nature genetics

Genomic and molecular characterization of esophageal squamous cell carcinoma

De-Chen Lin[1,2,8], Jia-Jie Hao[3,8], Yasunobu Nagata[4,8], Liang Xu[2,8], Li Shang[3], Xuan Meng[2], Yusuke Sato[4], Yusuke Okuno[4], Ana Maria Varela[2], Ling-Wen Ding[2], Manoj Garg[2], Li-Zhen Liu[2], Henry Yang[2], Dong Yin[5], Zhi-Zhou Shi[3], Yan-Yi Jiang[3], Wen-Yue Gu[3], Ting Gong[3], Yu Zhang[3], Xin Xu[3], Ori Kalid[6], Sharon Shacham[6], Seishi Ogawa[4], Ming-Rong Wang[3] & H Phillip Koeffler[1,2,7]

Esophageal squamous cell carcinoma (ESCC) is prevalent worldwide and particularly common in certain regions of Asia. Here we report the whole-exome or targeted deep sequencing of 139 paired ESCC cases, and analysis of somatic copy number variations (SCNV) of over 180 ESCCs. We identified previously uncharacterized mutated genes such as *FAT1*, *FAT2*, *ZNF750* and *KMT2D*, in addition to those already known (*TP53*, *PIK3CA* and *NOTCH1*). Further SCNV evaluation, immunohistochemistry and biological analysis suggested their functional relevance in ESCC. Notably, RTK-MAPK-PI3K pathways, cell cycle and epigenetic regulation are frequently dysregulated by multiple molecular mechanisms in this cancer. Our approaches also uncovered many druggable candidates, and XPO1 was further explored as a therapeutic target because it showed both gene mutation and protein overexpression. Our integrated study unmasks a number of novel genetic lesions in ESCC and provides an important molecular foundation for understanding esophageal tumors and developing therapeutic targets.

ESCC is one of the most common malignant diseases in the world and especially in China, where it is the fourth most common cause of cancer-related deaths[1]. Unlike that of cancers that have been extensively studied, such as breast and colon cancers, the outcome of ESCC remains unchanged during the last several decades, with a five-year survival rate ranging from 15% to 25% (ref. 2). We and others have revealed in ESCC frequent somatic copy number variations (SCNV) involving 3q26 (ref. 3), 9p21 (ref. 4), 11q13.3 (ref. 5) and 8q24.3 (ref. 6), as well as somatic mutations in *PIK3CA*[7], *TP53* (ref. 8) and *NOTCH1* (ref. 8). However, in general, understanding of the genomic abnormalities in this disease is limited to studies of small cohorts[4,6,7,9–12], including a recent whole-exome sequencing approach of 12 ESCCs[8]. Thus, a compelling need exists to extensively identify genomic abnormalities underlying ESCC, elucidate its molecular basis and guide the development of effective targeted therapies.

We first sequenced whole exomes (WES) of 20 matched ESCC germline and tumor pairs (discovery cohort, mean coverage 79×, **Supplementary Tables 1a** and **2a**). Transcriptome sequencing (RNA-seq) was also performed on 4 of these 20 tumors. A total of 1,186 nonsilent somatic mutations (affecting 1,042 genes) were identified (**Supplementary Table 3**), a mutation rate comparable to those of most adult solid tumors[13] (**Supplementary Fig. 1**). We extensively validated 362 candidate somatic mutations with Sanger sequencing (true-positive rate = 93.1%, **Supplementary Table 3**). Intratumoral clonality analysis showed that both biclonal and multiclonal signatures existed in ESCC (**Supplementary Fig. 2**). Cross comparing the WES with RNA-seq data from the same tumors revealed that 61% of the mutated genes were transcribed (**Supplementary Table 4**), which is comparable to the value reported for breast cancer[14].

To evaluate the prevalence of these mutated genes from discovery cohort, we sequenced all of their coding exons with 119 additional matched ESCC germline/tumors, as well as 10 ESCC cell lines (frequency cohort, mean coverage 111×, **Supplementary Tables 1b** and **2b**). To cover more comprehensively the mutational events in this disease, we also included an additional 277 genes that were discovered in the previous WES study of 12 ESCCs[8] or causally implicated in other human cancers (Cancer Gene Census; **Supplementary Table 5**). As a result, a total of 1,847 nonsilent somatic mutations were identified, with an average of 15 mutations per case (true-positive rate = 96.2%, **Fig. 1a**; **Supplementary Table 6**). Notably, the mutational spectrums from the discovery and frequency cohorts are almost identical (**Supplementary Fig. 3a**), suggesting that our targeted sequencing approach comprehensively unmasked most of the mutational events in DNA-coding regions in ESCC. Of note, trinucleotide-signature analysis suggested that DNA cytidine deaminase APOBEC3B is responsible for ESCC mutagenesis[15–17] (**Fig. 1b** and

[1]Cedars-Sinai Medical Center, Division of Hematology/Oncology, University of California Los Angeles School of Medicine, Los Angeles, California, USA. [2]Cancer Science Institute of Singapore, National University of Singapore, Singapore. [3]State Key Laboratory of Molecular Oncology, Cancer Institute (Hospital), Peking Union Medical College and Chinese Academy of Medical Sciences, Beijing, China. [4]Cancer Genomics Project, Graduate School of Medicine, University of Tokyo, Tokyo, Japan. [5]Medical Research Center, Sun Yat-Sen Memorial Hospital, Guangzhou, China. [6]Karyopharm Therapeutics, Natick, Massachusetts, USA. [7]National University Cancer Institute, National University Hospital Singapore, Singapore. [8]These authors contributed equally to this work. Correspondence should be addressed to M.-R.W. (wangmr2015@126.com) or D.-C.L. (dchlin11@gmail.com).

Received 28 August 2013; accepted 5 March 2014; published online 30 March 2014; doi:10.1038/ng.2935

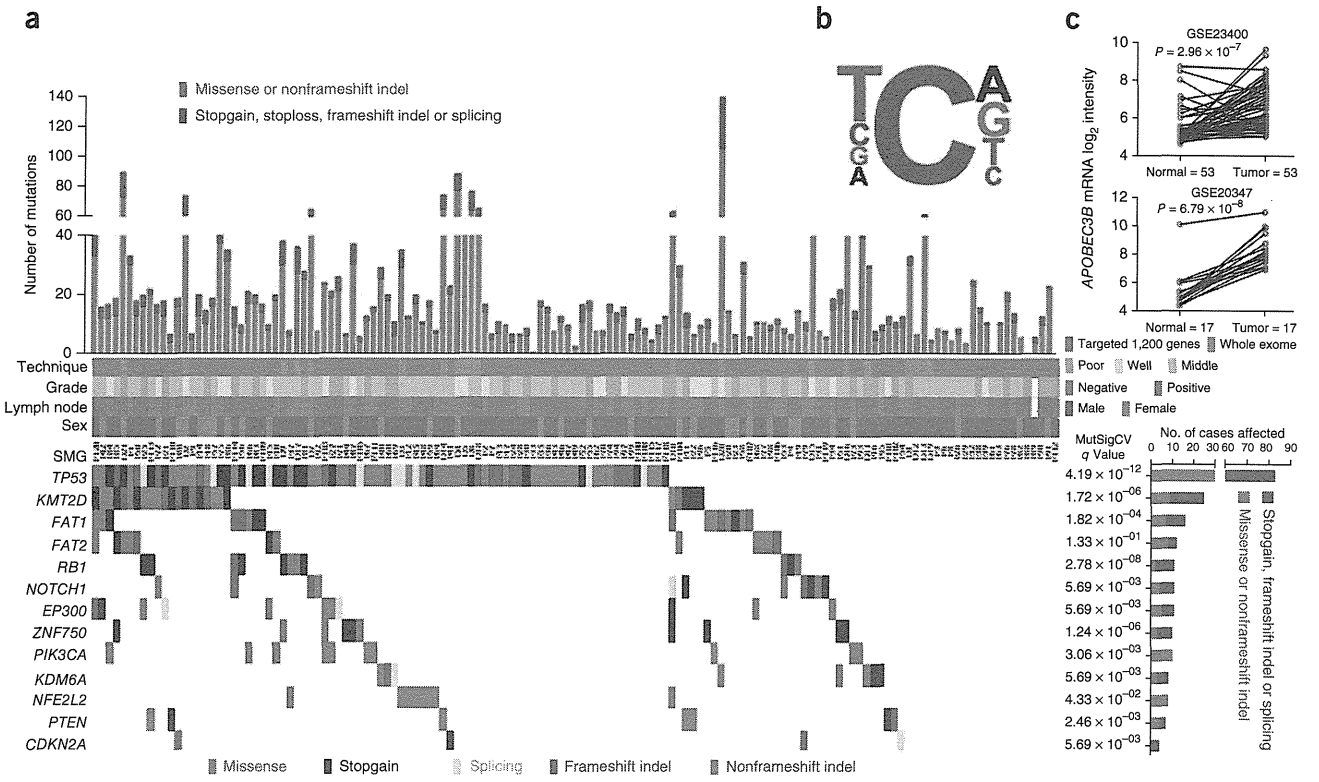

Figure 1 Mutation frequencies and signatures, and significantly mutated genes in 139 ESCCs. (**a**) The number of somatic mutations of each examined case (top), key clinical parameters (middle, see **Supplementary Table 2a,b**), and the significantly mutated genes (SMG) colored by the type of mutations and their mutational frequency (bottom). Columns correspond to examined cases. (**b**) Trinucleotide contexts of mutations occurring at cytosine nucleotides in ESCC. Font size of the bases at the 5′ and 3′ positions are proportional to their frequencies (**Supplementary Fig. 3b**). (**c**) *APOBEC3B* mRNA expression calculated from two data sets, GSE20347 (ref. 11) and GSE23400 (ref. 54), both of which examined cDNA microarray from matched normal and tumor ESCC cases.

Supplementary Fig. 3b), and indeed, APOBEC3B expression was clearly upregulated in ESCC tumors (**Fig. 1c**). We observed that 609 genes were mutated in two or more samples, with 62 genes mutated at a frequency over 5% (**Supplementary Fig. 3c**). To identify mutations conferring selective growth advantages ('driver mutations'), we applied the algorithm MutSigCV[13], which corrects for variation by incorporating patient-specific mutational spectrum and gene-specific background mutational burden and also by measuring gene expression and replication time. As a result, we calculated that 13 genes were significantly mutated (false-discovery rate $q < 0.2$). Notably, many of these mutated genes had not previously been implicated in ESCC.

To interrogate SCNV in ESCC, we examined 22 tumors with a SNP array (18 from the discovery cohort), as well as 59 samples with array CGH[18]. We further comprehensively analyzed three additional SNP-array data sets measuring primary ESCCs[4,11,12] (**Supplementary Table 7**), resulting in a total of 184 analyzable primary ESCC samples. We focused on focal SCNV, defined as narrow regions (typically <100 kb) showing high-amplitude copy number changes (Online Methods), which have a higher probability of containing cancer genes. This approach identified 14 recurrent focal SCNVs, with the most frequent amplification peak spanning the *CCND1* gene on 11q13.2 (**Supplementary Table 7**). Additional peaks involving important cancer genes such as *EGFR, MYC, KRAS* and *CDKN2A* were found. Notably, *FGFR1* was shown to be frequently amplified, which has not been reported before in ESCC. To confirm this observation, we examined an additional 53 ESCC tumors with fluorescence *in situ* hybridization (FISH) and found that *FGFR1* was amplified in 11 samples (**Fig. 2a** and **Supplementary Table 7**). Furthermore, with immunohistochemistry (IHC), we found that the FGFR1 protein was upregulated in 17.3% ESCC tumors (**Fig. 2b** and **Supplementary Table 8a**). Given that *FGFR* amplification is predictive of sensitivity to targeted inhibitors in several other solid tumors[19], our results suggest that FGFR1 is a potential therapeutic target in ESCC.

We next sought to understand dysregulated pathways in ESCC. As we previously reported protein alterations in ESCC using meta-analysis[20], here we also took into account protein overexpression evidence. Mitogen-activated protein kinase (MAPK) ($P = 0.0005$, **Fig. 2d**, **Supplementary Table 9a** and Online Methods) and phosphatidylinositol 3-kinase (PI3K) pathways ($P = 0.0004$) are augmented by multiple mechanisms: (i) amplification and overexpression of RTKs, KRAS and PIK3CA; (ii) activating mutations of *ERBB4* and *PIK3CA*; (iii) inactivating mutations of *PTEN*, *MAP3K13* and *MAP3K15*. In addition, *IL7R* amplification and *JAK1* mutations were identified, which will likely activate JAK-STAT3 signaling ($P = 0.0006$).We previously showed that p-STAT3 is elevated in ESCC[21], which transforms esophageal epithelial cells cooperatively with amplified *SOX2* (ref. 22). Cell cycle progression (**Fig. 2e**, $P = 1.63 \times 10^{-5}$) is altered mostly by *CCND1* amplification, *CDKN2A* deletion or mutation and *TP53* mutation. As a negative regulator of c-Myc, frequent *FBXW7* mutations were observed in our investigation (**Fig. 2c**), confirming a recent report of this gene in ESCC[8]. We next examined FBXW7 protein expression with IHC and found its mutation led to loss of the protein (**Fig. 2c**). Moreover, in an additional cohort ($n = 40$), we determined that FBXW7 protein was downregulated in 33% of tumors

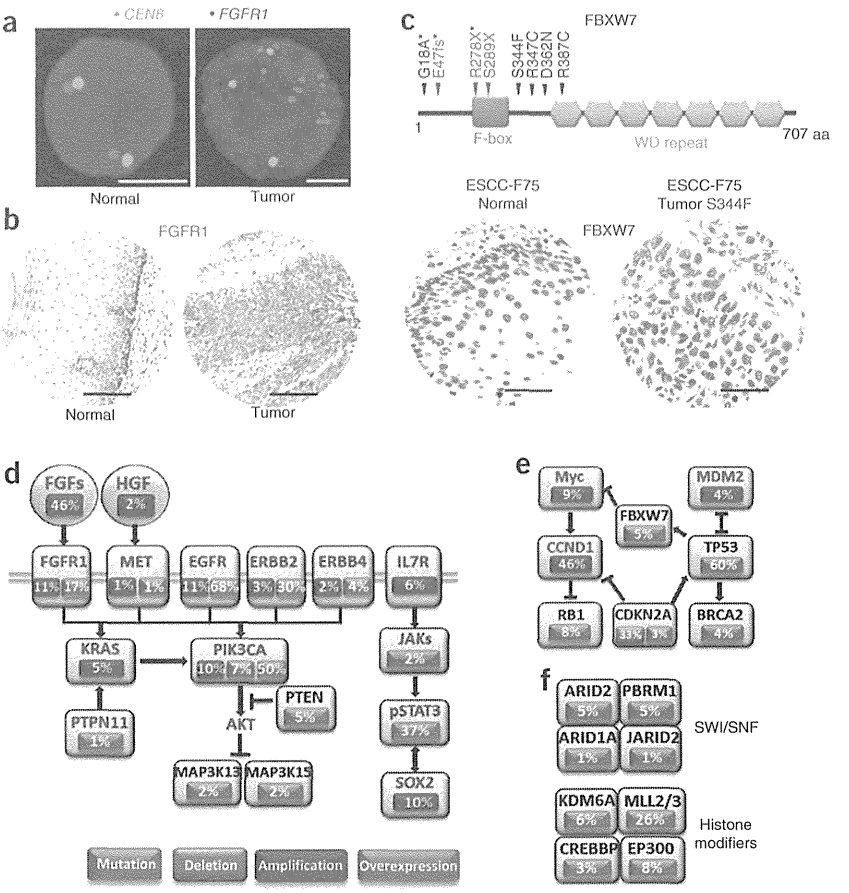

Figure 2 Dysregulated pathways in ESCC. (**a**) Representative FISH photos of an ESCC case with amplified *FGFR1*. Green signals label the centromere 8 probe (*CEN8*) and red signals label *FGFR1* gene probe. Scale bars, 5 μm. (**b**) Representative IHC photos of FGFR1 protein overexpression in ESCCs (additional cohort, 60 cases had matched adjacent normal epithelial tissues, see **Supplementary Table 8a**). Scale bars, 200 μm. (**c**) Top panel, schematics of protein alterations in FBXW7 caused by somatic mutations. Black, missense; red, stopgain (X) or frameshift indel (fs). An asterisk (*) indicates those alterations that were discovered by Agrawal *et al.*[8]. Conserved domains were mapped from UniProt. Bottom panel, representative FBXW7 IHC results of an ESCC case carrying *FBXW7* mutations (frequency and additional cohort, all cases had matched adjacent normal epithelial tissue, see **Supplementary Table 8b**). Scale bars, 100 μm. (**d–f**) Significantly dysregulated pathways colored by the type of alterations. Red font denotes a predicted activating alteration; black font denotes a predicted inactivating alteration. (**d**) RTK-MAPK-PI3K signaling. (**e**) G1-S cell cycle regulation. (**f**) Epigenetic modification.

(**Supplementary Fig. 4** and **Supplementary Table 8b**), further demonstrating its relevance in ESCC. Another prominent enrichment of mutated genes in ESCC are those implicated in epigenetic modifications (P = 0.0013, **Fig. 2f** and **Supplementary Table 9b**), such as members of the SWI/SNF complex (*ARID2* and *PBRM1*), histone methyltransferases *KMT2D* and *KMT2C*, and demethylase *KDM6A*.

ZNF750 is a poorly studied nuclear protein that is upregulated in differentiated skin keratinocytes[23,24]. We observed that *ZNF750* was significantly mutated in ESCC ($q = 1.24 \times 10^{-6}$, **Fig. 3a**). Notably, analysis of public data sets revealed that *ZNF750* is largely mutated in squamous cell carcinomas, with most of them presenting truncating mutations (**Supplementary Fig. 5b**). In line with this, ESCC harbors a much higher mutational burden affecting *ZNF750* than esophageal adenocarcinoma. The similar pattern was also observed when comparing lung SCC to lung adenocarcinoma. From Cancer Cell Line Encyclopedia (CCLE) results, we found that *ZNF750* mRNA showed higher expression in ESCC and upper aerodigestive squamous cell carcinoma (UASCC) than any other nonsquamous cancer cell lines (**Supplementary Fig. 5a**). These data suggest that *ZNF750* somatic mutations are biologically relevant in squamous cell malignancy. In addition, we found that *ZNF750* was focally deleted in 3.4% of ESCC tumors (**Fig. 3b**), and *ZNF750* mRNA expression was lower in esophageal tumors compared with normal tissue (**Fig. 3c**). Moreover, our IHC approach revealed that in normal esophageal epithelial, ZNF750 protein showed strong nuclear staining in the suprabasal layer of cells and above; whereas in ESCC tumors, ZNF750 showed much weaker expression (**Fig. 3d** and **Supplementary Table 8c**). Notably, in ESCC cells with wild-type endogenous ZNF750 expression, depletion of ZNF750 promoted cell proliferation (**Fig. 3e**), associated with a decreased expression of the genes implicated in late epithelial differentiation, whereas ectopic expression of ZNF750 led to the upregulation of these genes (**Supplementary Fig. 5c**). Moreover, 12-O-tetra-decanoylphorbol-13-acetate (TPA), a well-characterized differentiation-induction agent which has also been commonly used to promote ESCC differentiation[25,26], markedly enhanced ZNF750 expression (**Fig. 3f**), with a concomitant inhibition of cell proliferation (**Supplementary Fig. 5d**). Notably, ectopic expression of ZNF750 further promoted the TPA-induced growth suppression (**Fig. 3g**). Collectively, these results indicate that ZNF750 might function as a tumor suppressor in ESCC through regulating squamous cell differentiation.

The FAT family of proteins is comprised of FAT1, FAT2, FAT3 and FAT4, which are cadherin superfamily members encoded by genes homologous to the *Drosophila* gene *fat*. Very recently, *FAT1* was reported as a tumor suppressor in glioblastoma, colorectal cancer, and head and neck squamous cell carcinoma (HNSCC)[27]. However, the precise role of *FAT* genes in cancer still remains inconclusive and needs further characterization[28,29]. Our data revealed that ESCC harbored very frequent, mutually exclusive truncating mutations affecting *FAT1*, *FAT2* and *FAT3* compared to other solid tumors (**Fig. 4a,b** and **Supplementary Fig. 6a**). Among *FAT1*-mutated tumors, two samples were also analyzed with SNP array, and we discovered loss of heterozygosity of the *FAT1* gene in both tumors (**Supplementary Fig. 6b**), supporting Knudson's two-hit model. We next found that homozygous deletions of *FAT1* occurred in 3.4% of ESCCs (**Fig. 4c**). Furthermore, IHC staining demonstrated that FAT1 protein expression was downregulated in ESCC (**Fig. 4d**). To study the function of *FAT* gene inactivation in ESCC, we first silenced wild-type FAT1 expression with siRNA, and observed an increase in cell proliferation (**Fig. 4e**). On the other hand, ectopic expression of FAT1 cDNA[27]

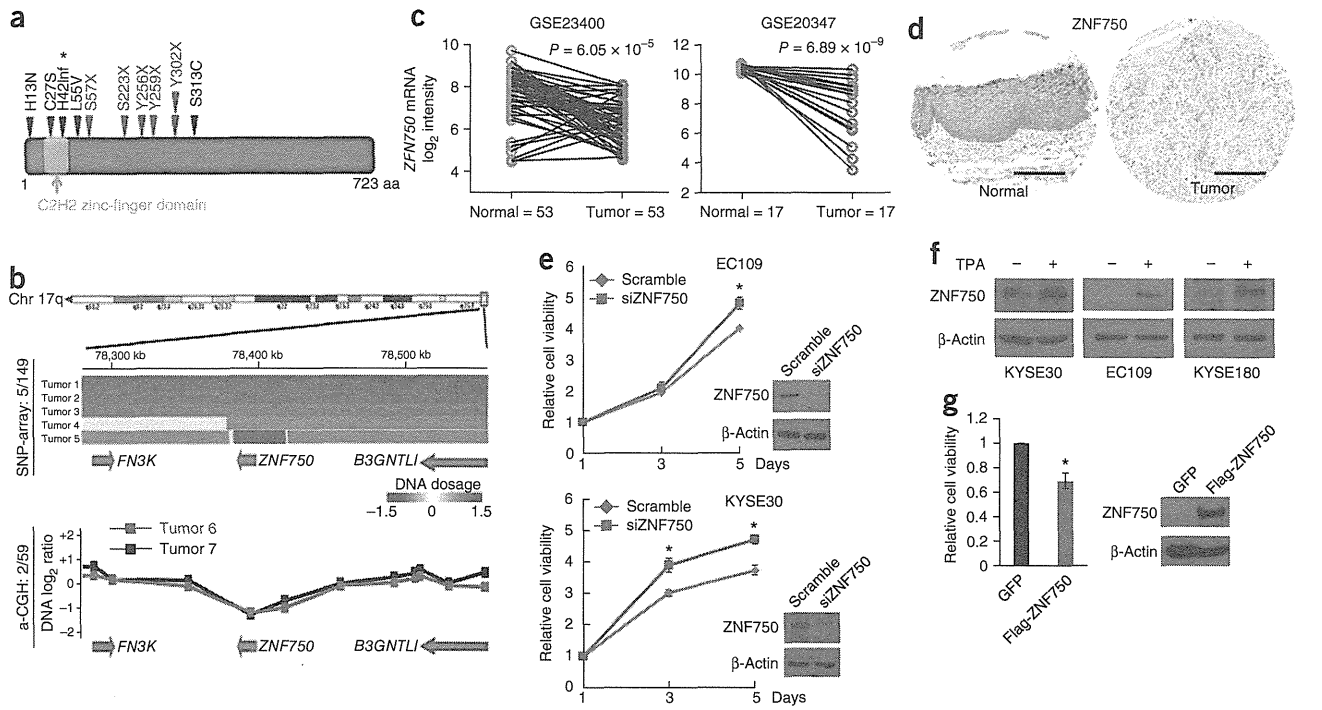

Figure 3 Identification of ZNF750 as a recessive cancer gene newly implicated in ESCC. (**a**) Schematics of protein alterations in ZNF750 caused by somatic mutations. Black, missense or inframe (inf); red, stopgain (X). An asterisk (*) indicates those discovered by Agrawal *et al.*[8]. Conserved domains were mapped from UniProt. (**b**) Top, IGV (Integrative Genomics Viewer) heatmap showing loss of *ZNF750* copy number identified from 149 ESCC SNP-array data; bottom, segmentation map of two tumors with *ZNF750* deletions from 59 ESCCs examined with array CGH. (**c**) *ZNF750* mRNA expression calculated from GSE20347 (ref. 11) and GSE23400 (ref. 54). (**d**) Representative IHC photos of ZNF750 protein expression in ESCCs (additional cohort, all cases had matched adjacent normal epithelial tissues, see **Supplementary Table 8c**). Scale bars, 400 μm. (**e**) Short-term cell proliferation assays of EC109 and KYSE30 cells transfected with either siRNAs against ZNF750 (si-ZNF750) or control siRNA (Scramble). Data represent mean ± s.d.; $n = 3$. (**f**) ESCC cells were treated with TPA (100 nM) for 24 h and lysates were analyzed by protein blot. (**g**) Under TPA (100 nM) treatment, short-term cell proliferation assay of KYSE30 cells ectopically expressing either GFP or ZNF750 proteins. Data represent mean ± s.d.; $n = 3$. Immunoblots of ZNF750 protein expression are shown with β-actin as a loading control. *$P < 0.05$.

significantly inhibited both cell proliferation ($P = 0.001$) and colony formation in soft agar ($P = 0.019$, **Supplementary Fig. 7**). Depletion of FAT2 with shRNA promoted ESCC growth *in vivo* (**Fig. 4f,g**). Together, the presence of mutations and alterations in protein expression with functional consequences strongly suggest that *FAT1* and *FAT2* likely encode tumor suppressors that are frequently disrupted in ESCC.

In mammalian cells, the chief mediator of protein nuclear export is exportin 1 (XPO1). Because XPO1 exports a number of tumor suppressors, targeting it has been considered as an antineoplastic approach[30]. We found one missense substitution, D624G, affecting *XPO1*. Notably, this mutation is identical to the one discovered in chronic lymphocytic leukemia[31]. Structural modeling analysis revealed that Asp624 is part of the site at which XPO1 binds conventional cargo, such as Snurportin[32,33]; for example, Asp624 forms a salt bridge with Snurportin's Lys144 (**Fig. 5a**). D624G substitution presumably reduces the affinity of interactions owing to loss of the salt bridge. This alteration may accelerate the turnover of XPO1 from the 'bound' to 'unbound' state and enhance its exporting efficiency. We next analyzed the expression of XPO1's mRNA and protein and found that they were frequently overexpressed in ESCC tumor samples (**Fig. 5b,c**). Moreover, XPO1 overexpression positively correlated with larger tumor size ($P = 0.016$, **Supplementary Table 8d**). Notably, the *XPO1*-mutated tumor also showed upregulated protein expression compared with the matched adjacent normal esophageal epithelium, indicating a gain-of-function phenotype (**Fig. 5b**). We next silenced *XPO1* gene expression with shRNA, and noticed the induction of apoptosis (as evidenced by cleaved PARP) and retardation of cell proliferation (**Fig. 5d,e**). To explore whether XPO1 is druggable in ESCC, we treated ESCC cells with a newly developed oral, small-molecule inhibitor, KPT-330, which specifically blocks XPO1 function by binding to the active-site Cys528 (refs. 34–36). Submicromolar concentrations of KPT-330 inhibited ESCC cell proliferation and induced marked apoptosis (**Fig. 5f,g**). Inhibition of XPO1 with either shRNA or KPT-330 altered the expression of its known cargos (such as P53), as well as indirect targets including Cyclin D1, c-Myc, PUMA and BIM, which might be a result of various mechanisms that we and others have recently identified[37–43] (**Fig. 5e,h**). Given that frequent overexpression of XPO1 protein is clinically relevant[44–47] and functionally contributes to the cellular malignant phenotype, targeting XPO1 in those patients with XPO1 upregulation might offer potential benefits in ESCC.

In an effort to identify therapeutic targets in ESCC, we correlated genomic mutations, amplifications, and mRNA and protein upregulation[48–51] in both primary tumors and cancer cell lines, with novel targeted therapeutic approaches. We chose those targeting approaches that have been approved for clinical use[52,53] or are under evaluation in clinical trials (see URLs section below). As a result, we identified 31 genes with alterations that can potentially be targeted for therapy in ESCC. Recurrent candidate druggable targets included

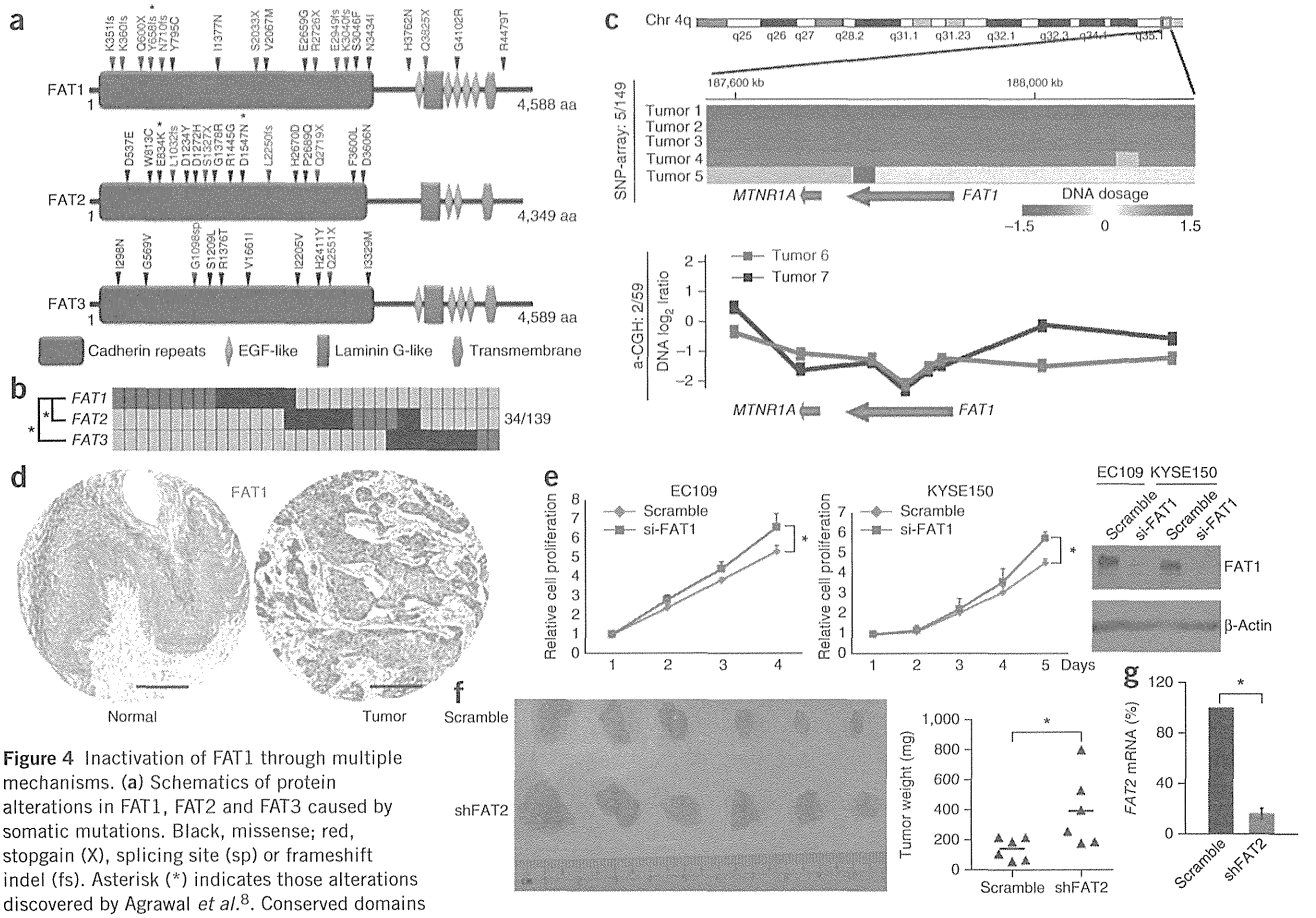

Figure 4 Inactivation of FAT1 through multiple mechanisms. (**a**) Schematics of protein alterations in FAT1, FAT2 and FAT3 caused by somatic mutations. Black, missense; red, stopgain (X), splicing site (sp) or frameshift indel (fs). Asterisk (*) indicates those alterations discovered by Agrawal *et al.*[8]. Conserved domains were mapped from UniProt. (**b**) Mutually exclusive analysis of *FAT1*, *FAT2* and *FAT3* mutations. Columns correspond to examined cases. Black, missense; red, stopgain, splicing site or frameshift indel. $^*P < 0.01$. (**c**) Top, IGV heatmap showing loss of *FAT1* copy number identified from 149 ESCC SNP-array data; bottom, segmentation map of two tumors with *FAT1* deletions from 59 ESCC array-CGH data. (**d**) Representative IHC photos of FAT1 protein expression in ESCCs (additional cohort, all 18 cases had matched adjacent normal epithelial tissues, see **Supplementary Table 8e**). Scale bars, 400 μm. (**e**) Short-term cell proliferation was measured in EC109 and KYSE150 cells transfected with either siRNAs against FAT1 (si-FAT1) or control (Scramble). Values represent mean ± s.d.; $n = 4$. Protein blot shows FAT1 expression in indicated samples with β-Actin as a loading control. (**f**) KYSE150 cells stably expressing either control shRNA (Scramble) or shRNA targeting FAT2 (shFAT2) were injected subcutaneously on the upper flanks of NOD/SCID mice. After 19 d, mice were killed, and the tumors were analyzed. (**g**) Relative expression of mRNAs of FAT2 quantified with q-PCR in either Scramble or shFAT2 KYSE150 cells. Value represent mean ± s.d.; $n = 3$. $^*P < 0.05$.

ERBB, HDAC and PI3K family, XPO1, FGFR1, TP53, JAK-STAT3 and MTOR-RPS6K signaling (**Supplementary Tables 10–12**). Importantly, most of the targets and pathways discovered here have not previously been considered as targets in ESCC. These results suggest that many potential therapeutic targets exist in ESCC that need further investigation.

In summary, we report the mutational landscape of 139 ESCCs as well as an SCNV overview of 184 ESCC cases. A number of mutated genes and altered pathways not previously associated with ESCC were identified with statistical and biological evidence of growth selection, indicating that they likely contribute to esophageal tumorigenesis. In addition to XPO1, our analysis proposes many potential therapeutic targets, which offer opportunities to address a typically chemo-resistant cancer.

URLs. dbSNP, http://www.ncbi.nlm.nih.gov/projects/SNP/; 1000 Genomes Project, http://www.1000genomes.org/; Copy Number Analyzer for Affymetrix GeneChip, http://www.genome.umin.jp/; MutSigCV, http://www.broadinstitute.org/cancer/cga/mutsig; TCGA, http://cancergenome.nih.gov/; COSMIC, http://cancer.sanger.ac.uk/cancergenome/projects/cosmic/; Clinical trials database, http://clinicaltrials.gov/; CCLE, http://www.broadinstitute.org/ccle/home; Tumorscape, http://www.broadinstitute.org/tumorscape/pages/portalHome.jsf; Integrated Genomics Viewer, http://www.broadinstitute.org/igv; UniProt, http://www.uniprot.org/; BRB-CGH tools, http://linus.nci.nih.gov/BRB-ArrayTools.html; MD-SeeGH, http://www.flintbox.com/public/project/579; Sequence Read Archive, http://www.ncbi.nlm.nih.gov/sra.

METHODS

Methods and any associated references are available in the online version of the paper.

Accession codes. Deep sequencing files have been deposited into Sequence Read Archive under accession number SRP033394.

Note: Any Supplementary Information and Source Data files are available in the online version of the paper.

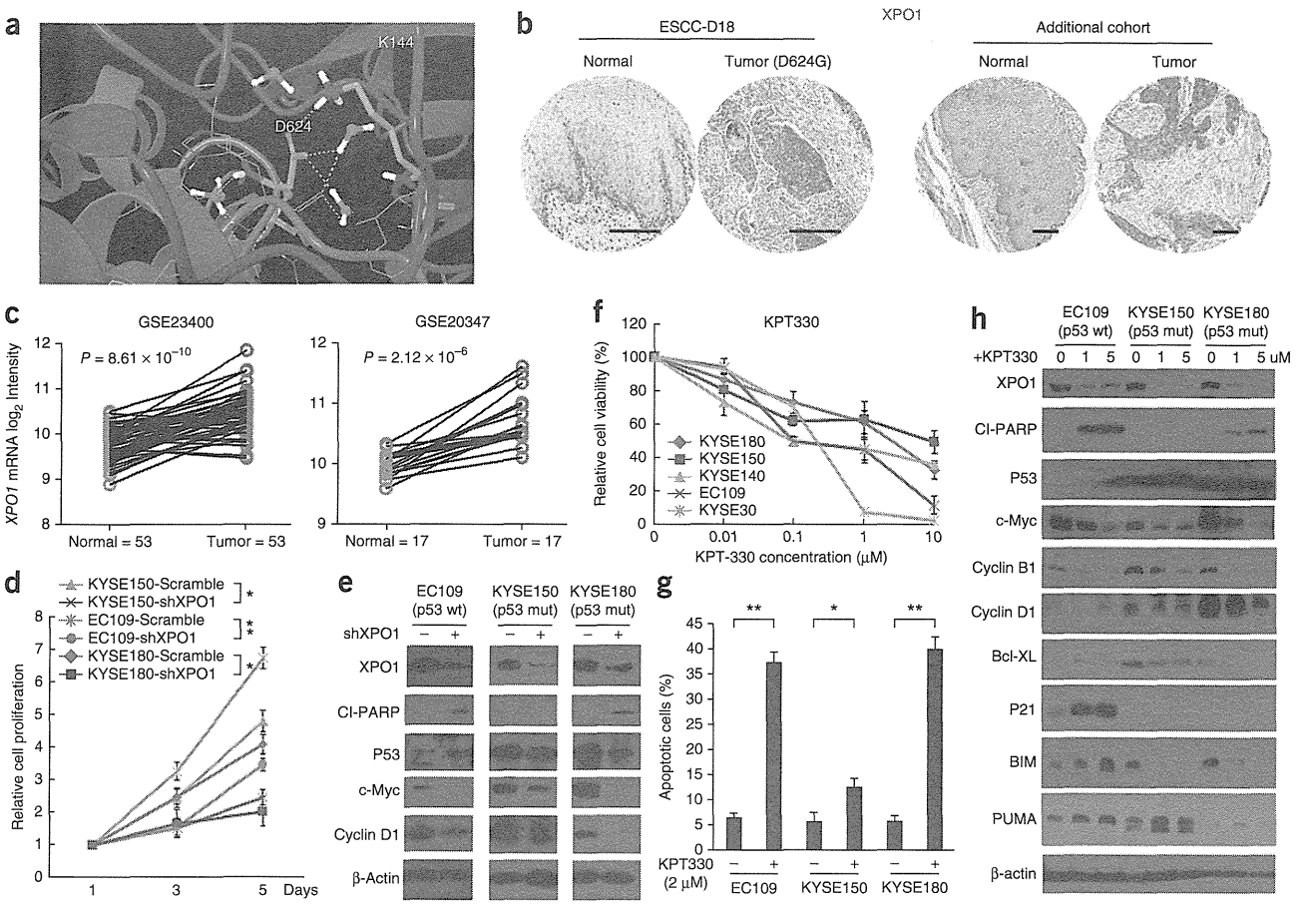

Figure 5 Targeting XPO1 in ESCC. (**a**) Crystal structural modeling of D624G alteration in XPO1 protein (gray ribbon) and its relationship with Snurportin (red ribbon). Dashed yellow lines represent hydrogen bonds. (**b**) Representative IHC photos of XPO1 protein expression in ESCCs (ESCC-D18 was from the discovery cohort; the rest of the cases were from the additional cohort, all cases had matched adjacent normal epithelial tissues, see **Supplementary Table 8d**). Scale bars, 200 μm. (**c**) XPO1 mRNA expression examined from GSE20347 (ref. 11) and GSE23400 (ref. 54). (**d**,**e**) ESCC cells were infected with lentivirus encoding shRNA against either XPO1 (shXPO1) or control shRNA (Scramble), and their proliferation was measured (**d**), and cell lysates were analyzed by protein blot with indicated antibodies (**e**). (**f**–**h**) ESCC cells were treated with KPT-330 at indicated concentrations for 72 h, and cell proliferation and apoptosis (**g**) were measured, and cell lysates were subjected to protein blot analysis with indicated antibodies and β-actin as a loading control (**h**). Values in **d**, **f** and **g** represent mean ± s.d., $n = 4$. $^{**}P < 0.01$; $^{*}P < 0.05$.

ACKNOWLEDGMENTS

We thank P. Tan and Z. Zang for generously sharing related facilities. We also thank B. Koegler and S. Koegler for their generous support. This work is supported by National High-Tech R&D Program of China 2012AA02A503 and 2012AA02A209 (M.-R.W.), National Natural Science Foundation of China 81330052 (M.-R.W.), US National Institutes of Health grant R01CA026038-35 (H.P.K.), National Research Foundation Singapore and the Singapore Ministry of Education under the Research Centers of Excellence initiative (H.P.K.), and Singapore Ministry of Health's National Medical Research Council under its Singapore Translational Research (STaR) Investigator Award to H.P.K.

AUTHOR CONTRIBUTIONS

D.-C.L., M.-R.W. and H.P.K. designed the study and wrote the manuscript. D.-C.L., J.-J.H., Y.N., Y.S., Y.O., X.M., L.X., A.M.V., L.-W.D. and M.G. performed experiments. D.Y, J.-J.H., Z.-Z.S., L.S., Y.-Y.J., W.-Y.G., T.G., Y.Z. and X.X. coordinated sample collection and processing. O.K. and S.S. provided KPT-330 and structurally analyzed *XPO1* point mutation. D.-C.L., J.-J.H., Y.N., S.O., M.-R.W. and H.P.K. analyzed and discussed the data. Y.N., H.Y., L.-Z.L., Y.S. and Y.O. performed bioinformatical analysis.

COMPETING FINANCIAL INTERESTS

The authors declare competing financial interests: details accompany the online version of the paper.

1. Zhao, P., Dai, M., Chen, W. & Li, N. Cancer trends in China. *Jpn. J. Clin. Oncol.* **40**, 281–285 (2010).
2. Pennathur, A., Gibson, M.K., Jobe, B.A. & Luketich, J.D. Oesophageal carcinoma. *Lancet* **381**, 400–412 (2013).
3. Yang, Y.L. *et al.* Amplification of PRKCI, located in 3q26, is associated with lymph node metastasis in esophageal squamous cell carcinoma. *Genes Chromosom. Cancer* **47**, 127–136 (2008).
4. Bass, A.J. *et al.* SOX2 is an amplified lineage-survival oncogene in lung and esophageal squamous cell carcinomas. *Nat. Genet.* **41**, 1238–1242 (2009).
5. Luo, M.L. *et al.* Amplification and overexpression of CTTN (EMS1) contribute to the metastasis of esophageal squamous cell carcinoma by promoting cell migration and anoikis resistance. *Cancer Res.* **66**, 11690–11699 (2006).
6. Hu, N. *et al.* Genomic characterization of esophageal squamous cell carcinoma from a high-risk population in China. *Cancer Res.* **69**, 5908–5917 (2009).
7. Shigaki, H. *et al.* PIK3CA mutation is associated with a favorable prognosis among patients with curatively resected esophageal squamous cell carcinoma. *Clin. Cancer Res.* **19**, 2451–2459 (2013).
8. Agrawal, N. *et al.* Comparative genomic analysis of esophageal adenocarcinoma and squamous cell carcinoma. *Cancer Discov.* **2**, 899–905 (2012).

9. Shi, Z.Z. *et al.* Genomic alterations with impact on survival in esophageal squamous cell carcinoma identified by array comparative genomic hybridization. *Genes Chromosom. Cancer* **50**, 518–526 (2011).
10. Hirasaki, S. *et al.* BAC clones related to prognosis in patients with esophageal squamous carcinoma: an array comparative genomic hybridization study. *Oncologist* **12**, 406–417 (2007).
11. Hu, N. *et al.* Genome wide analysis of DNA copy number neutral loss of heterozygosity (CNNLOH) and its relation to gene expression in esophageal squamous cell carcinoma. *BMC Genomics* **11**, 576 (2010).
12. Beroukhim, R. *et al.* The landscape of somatic copy-number alteration across human cancers. *Nature* **463**, 899–905 (2010).
13. Lawrence, M.S. *et al.* Mutational heterogeneity in cancer and the search for new cancer-associated genes. *Nature* **499**, 214–218 (2013).
14. Shah, S.P. *et al.* The clonal and mutational evolution spectrum of primary triple-negative breast cancers. *Nature* **486**, 395–399 (2012).
15. Burns, M.B., Temiz, N.A. & Harris, R.S. Evidence for APOBEC3B mutagenesis in multiple human cancers. *Nat. Genet.* **45**, 977–983 (2013).
16. Burns, M.B. *et al.* APOBEC3B is an enzymatic source of mutation in breast cancer. *Nature* **494**, 366–370 (2013).
17. Roberts, S.A. *et al.* An APOBEC cytidine deaminase mutagenesis pattern is widespread in human cancers. *Nat. Genet.* **45**, 970–976 (2013).
18. Shi, Z.Z. *et al.* Consistent and differential genetic aberrations between esophageal dysplasia and squamous cell carcinoma detected by array comparative genomic hybridization. *Clin. Cancer Res.* **19**, 5867–5878 (2013).
19. Guagnano, V. *et al.* FGFR genetic alterations predict for sensitivity to NVP-BGJ398, a selective pan-FGFR inhibitor. *Cancer Discov.* **2**, 1118–1133 (2012).
20. Lin, D.C., Du, X.L. & Wang, M.R. Protein alterations in ESCC and clinical implications: a review. *Dis. Esophagus* **22**, 9–20 (2009).
21. Zhang, Y. *et al.* Reciprocal activation between PLK1 and Stat3 contributes to survival and proliferation of esophageal cancer cells. *Gastroenterology* **142**, 521–530 (2012).
22. Liu, K. *et al.* Sox2 cooperates with inflammation-mediated Stat3 activation in the malignant transformation of foregut basal progenitor cells. *Cell Stem Cell* **12**, 304–315 (2013).
23. Cohen, I. *et al.* ZNF750 is expressed in differentiated keratinocytes and regulates epidermal late differentiation genes. *PLoS ONE* **7**, e42628 (2012).
24. Sen, G.L. *et al.* ZNF750 is a p63 target gene that induces KLF4 to drive terminal epidermal differentiation. *Dev. Cell* **22**, 669–677 (2012).
25. Yu, X. *et al.* Differentiation-associated genes regulated by TPA-induced c-Jun expression via a PKC/JNK pathway in KYSE450 cells. *Biochem. Biophys. Res. Commun.* **342**, 286–292 (2006).
26. Chen, H. *et al.* S100A14 is a novel modulator of terminal differentiation of esophageal squamous cell carcinoma. *Mol. Cancer Res.* **11**, 1542–1553 (2013).
27. Morris, L.G. *et al.* Recurrent somatic mutation of FAT1 in multiple human cancers leads to aberrant Wnt activation. *Nat. Genet.* **45**, 253–261 (2013).
28. Dikshit, B. *et al.* FAT1 acts as an upstream regulator of oncogenic and inflammatory pathways, via PDCD4, in glioma cells. *Oncogene* **32**, 3798–3808 (2013).
29. de Bock, C.E. *et al.* The Fat1 cadherin is overexpressed and an independent prognostic factor for survival in paired diagnosis-relapse samples of precursor B-cell acute lymphoblastic leukemia. *Leukemia* **26**, 918–926 (2012).
30. Turner, J.G., Dawson, J. & Sullivan, D.M. Nuclear export of proteins and drug resistance in cancer. *Biochem. Pharmacol.* **83**, 1021–1032 (2012).
31. Landau, D.A. *et al.* Evolution and impact of subclonal mutations in chronic lymphocytic leukemia. *Cell* **152**, 714–726 (2013).
32. Paraskeva, E. *et al.* CRM1-mediated recycling of snurportin 1 to the cytoplasm. *J. Cell Biol.* **145**, 255–264 (1999).
33. Monecke, T. *et al.* Crystal structure of the nuclear export receptor CRM1 in complex with Snurportin1 and RanGTP. *Science* **324**, 1087–1091 (2009).
34. Ranganathan, P. *et al.* Preclinical activity of a novel CRM1 inhibitor in acute myeloid leukemia. *Blood* **120**, 1765–1773 (2012).
35. Etchin, J. *et al.* KPT-330 inhibitor of CRM1 (XPO1)-mediated nuclear export has selective anti-leukaemic activity in preclinical models of T-cell acute lymphoblastic leukaemia and acute myeloid leukaemia. *Br. J. Haematol.* **161**, 117–127 (2013).
36. Etchin, J. *et al.* Antileukemic activity of nuclear export inhibitors that spare normal hematopoietic cells. *Leukemia* **27**, 66–74 (2013).
37. Chen, L., Fischle, W., Verdin, E. & Greene, W.C. Duration of nuclear NF-kappaB action regulated by reversible acetylation. *Science* **293**, 1653–1657 (2001).
38. Kanezaki, R. *et al.* Transcription factor BACH1 is recruited to the nucleus by its novel alternative spliced isoform. *J. Biol. Chem.* **276**, 7278–7284 (2001).
39. Kim, J.Y. & Casaccia, P. HDAC1 in axonal degeneration: a matter of subcellular localization. *Cell Cycle* **9**, 3680–3684 (2010).
40. Lapalombella, R. *et al.* Selective inhibitors of nuclear export show that CRM1/XPO1 is a target in chronic lymphocytic leukemia. *Blood* **120**, 4621–4634 (2012).
41. Schmidt, J. *et al.* Genome-wide studies in multiple myeloma identify XPO1/CRM1 as a critical target validated using the selective nuclear export inhibitor KPT-276. *Leukemia* **27**, 2357–2365 (2013).
42. Walker, C.J. *et al.* Preclinical and clinical efficacy of XPO1/CRM1 inhibition by the karyopherin inhibitor KPT-330 in Ph+ leukemias. *Blood* **122**, 3034–3044 (2013).
43. Tai, Y.T. *et al.* CRM1 inhibition induces tumor cell cytotoxicity and impairs osteoclastogenesis in multiple myeloma: molecular mechanisms and therapeutic implications. *Leukemia* **28**, 155–165 (2014).
44. Huang, W.Y. *et al.* Prognostic value of CRM1 in pancreas cancer. *Clin. Invest. Med.* **32**, E315 (2009).
45. Kojima, K. *et al.* Prognostic impact and targeting of CRM1 in acute myeloid leukemia. *Blood* **121**, 4166–4174 (2013).
46. Noske, A. *et al.* Expression of the nuclear export protein chromosomal region maintenance/exportin 1/Xpo1 is a prognostic factor in human ovarian cancer. *Cancer* **112**, 1733–1743 (2008).
47. Shen, A. *et al.* Expression of CRM1 in human gliomas and its significance in p27 expression and clinical prognosis. *Neurosurgery* **65**, 153–159, discussion 159–160 (2009).
48. Wei, Q. *et al.* EGFR, HER2 and HER3 expression in esophageal primary tumours and corresponding metastases. *Int. J. Oncol.* **31**, 493–499 (2007).
49. Sato-Kuwabara, Y., Neves, J.I., Fregnani, J.H., Sallum, R.A. & Soares, F.A. Evaluation of gene amplification and protein expression of HER-2/neu in esophageal squamous cell carcinoma using fluorescence in situ hybridization (FISH) and immunohistochemistry. *BMC Cancer* **9**, 6 (2009).
50. Boone, J. *et al.* mTOR in squamous cell carcinoma of the oesophagus: a potential target for molecular therapy? *J. Clin. Pathol.* **61**, 909–913 (2008).
51. Akagi, I. *et al.* Overexpression of PIK3CA is associated with lymph node metastasis in esophageal squamous cell carcinoma. *Int. J. Oncol.* **34**, 767–775 (2009).
52. Garnett, M.J. *et al.* Systematic identification of genomic markers of drug sensitivity in cancer cells. *Nature* **483**, 570–575 (2012).
53. Somaiah, N. & Simon, G.R. Molecular targeted agents and biologic therapies for lung cancer. *J. Thorac. Oncol.* **6**, S1758–S1785 (2011).
54. Su, H. *et al.* Global gene expression profiling and validation in esophageal squamous cell carcinoma and its association with clinical phenotypes. *Clin. Cancer Res.* **17**, 2955–2966 (2011).